最初に，アストロサイトが活性化する過程について考えてみたい。前述のとおり，Aβはグリア細胞を活性化することが示唆される。その機序として考えられるのは，Aβがアストロサイト内のカルシウム動態に変化をもたらすためである可能性がある[6]。細胞内のカルシウム濃度が上昇すると，カルシウム依存性の経路のスイッチが入るが，その経路の1つとしてカルシニューリンを介した経路が挙げられる。そこで今回，アストロサイトのカルシニューリンに着目して行った実験について紹介したい。また，実際のAD患者脳でのアストロサイト内のカルシニューリンに関しても触れていく。

次に，活性化されたアストロサイトが放出する因子について述べる。アストロサイトは活性化すると，ミクログリア同様，様々なサイトカインや因子を放出することが知られている[7]。そこで，Aβ刺激によりアストロサイトが放出する因子を，後述するantibody arrayという手法を用いて検索した。得られた結果の中で，最も顕著に放出が認められたインスリン様成長因子（IGF）結合タンパク質-3（IGFBP-3）という因子に着目した。IGFBP-3は文字どおりIGFに結合するタンパク質で，IGFの生理活性を制御する働きがあると考えられている。その性質から，アルツハイマー病理の1つの側面として報告されている，後述の「IGF抵抗性」[8]に深く関与しうる因子である。最後に，IGFBP-3が，AD患者脳においてニューロンの細胞死にどのように関与しているかの仮説を紹介する。

Ⅰ．Aβによるアストロサイト内のカルシウム動態変化

Aβによってアストロサイトのカルシウム濃度が上昇する報告はこれまでにもいくつかなされている。Talantovaらによると[9]，Fura2を用いた実験で，Aβを負荷するとアストロサイト内のカルシウム濃度が上昇し，グルタミン酸の放出が促される。マウスの初代培養アストロサイトを用いて細胞内カルシウム濃度の変化を見た自験例を**図❶**に示す。通常，アストロサイトでは，oscillationといって細胞内カルシウム濃度が上昇しては元に戻るといった動態を示すが，Aβを負荷すると対照ペプチドを加えた場合に比べ，図に示すようにそのoscillationの振幅が増大し，一時的にカルシウム濃度が著明に増加することが明らかになった。これにより，脳内においても，放出されたAβがアストロサイト内のカルシウム濃度を一過性に激しく上昇させることが推定された。

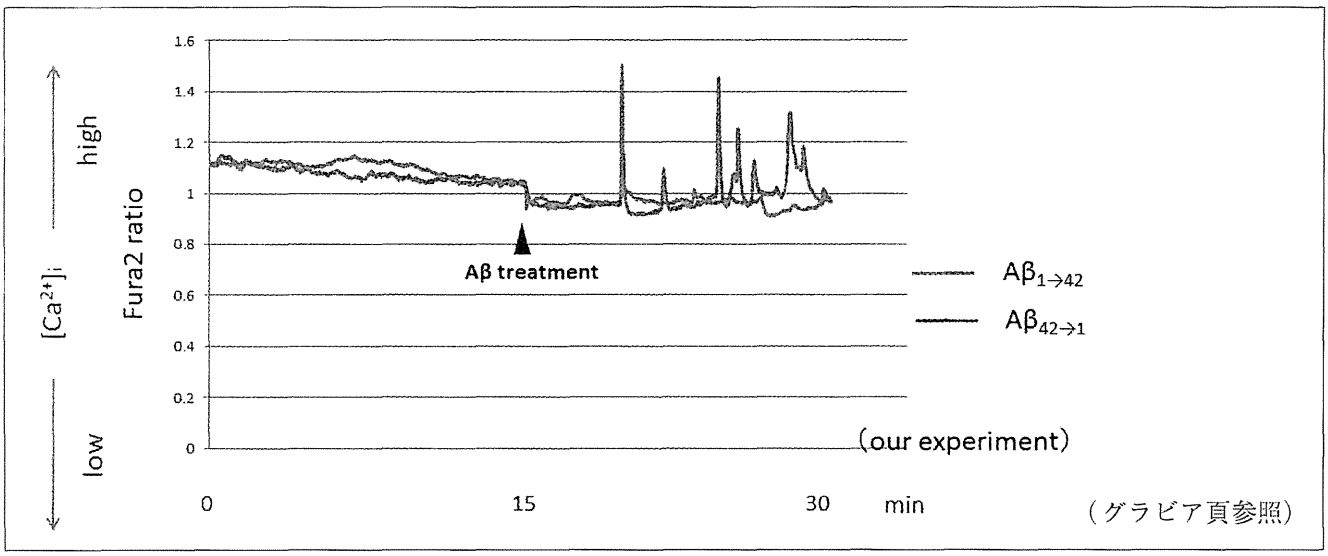

図❶　Aβによりアストロサイト内カルシウム濃度の上昇を認める

Aβによるアストロサイト内のカルシウム動態を調べた。マウス初代培養アストロサイトにAβとコントロールを負荷し，細胞内カルシウム濃度の変化を測定した。コントロール（青色）に比べて，Aβ（赤色）を加えた場合，アストロサイト内のカルシウム濃度が激しく上昇しては元に戻る（oscillation）ことがわかる。

Ⅱ. カルシウム依存性カスケードであるカルシニューリンとAD病

カルシウムを介して細胞内のシグナル伝達を行う経路はいくつか知られているが，われわれはその中でカルシウム結合タンパク質であるカルシニューリンに着目した。カルシニューリンはカルシウムおよびカルモジュリンと結合すると，その自己制御ドメインがはずれ，活性型に変化し，脱リン酸化作用を呈する。カルシニューリンの下流にはNFATなどが知られており，最終的に様々な転写の活性を促す[10]。カルシニューリンはその名のとおり，もともとはニューロンに多く存在すると考えられていたが，アストロサイトなどその他のグリア細胞内にも存在する[11]。また，AD患者脳とカルシニューリンに関する報告も今までいくつかなされている[12]。われわれは，アストロサイト内で活性化するカルシニューリンの関与を検討するために，AD患者脳切片を用いてアストロサイト内のカルシニューリンの蛍光免疫染色を行った。図❷に示すように，AD患者脳では，アストロサイト細胞質内のカルシニューリンの発現が増加しているのと比べ，対照脳ではアストロサイト内にはあまり発現していないことがわかる。図❷Bのグラフはそれを定量化したもので，アストロサイト内にカルシニューリンが発現している割合を示すが，共局在しているアストロサイトは有意に増加していることがわかる。これらの結果よりAD脳においてもカルシニューリンの発現が増大していることが強く示唆された。

Ⅲ. アストロサイトから放出される様々な因子

グリア細胞のグリアという名前は，接着剤として使われる「にかわ」を表すギリシア語に由来する。その名の示すように，これまでは単に「空間を埋める間質」とみなされてきたのだが，最近ではニューロンに対し様々な因子を供給していることがわかってきている。免疫を担当するミクログリアは当然，サイトカインをはじめとして様々な免疫系因子を放出しているが，アストロサイトも同様に各種の因子を放出していることが知られるようになった。そこでわれわれは，ADにおいて活性化したアストロサイトがニューロンに及ぼす影響を考えるにあたって，こうした因子が関係するのではないかという仮説をたてた。そのために，マウス初代培養アストロサイトを用いて，Aβに反応して放出される因子をantibody arrayという方法を用いて検索した。antibody array（RayBio® biotin label-based cytokine antibody array）は，100種類以上の決まった因子に対する抗体がメンブレンにブロットされており，アストロサイトにAβ

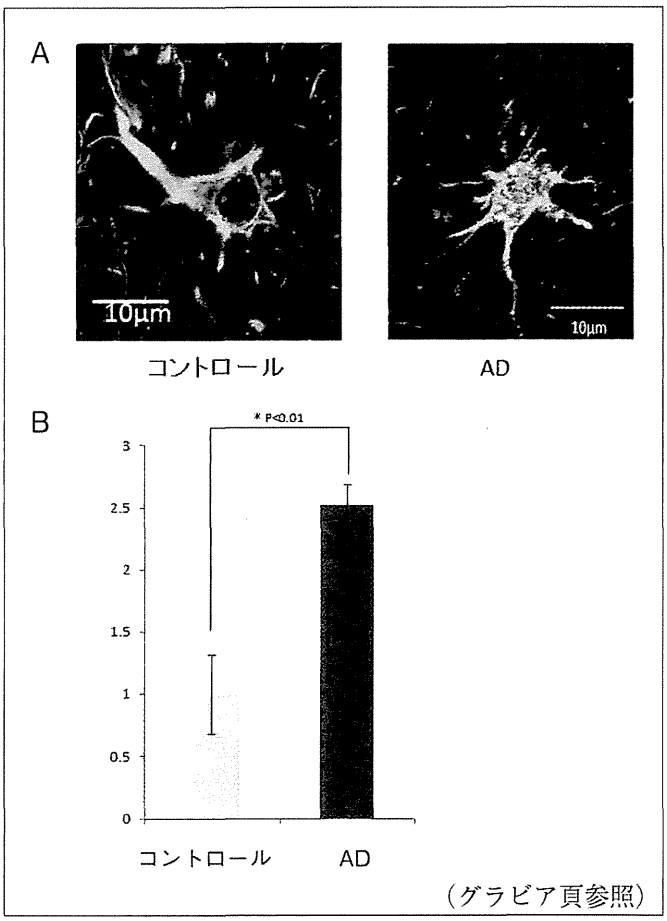

（グラビア頁参照）

図❷ アストロサイト内のカルシニューリン発現

A. ヒト脳の蛍光免疫染色である。緑色に染色された細胞がアストロサイトで，赤色でカルシニューリンが染色されている。コントロールでは，アストロサイト内にカルシニューリンはほとんど認めないのに対して，AD脳では，アストロサイト内にカルシニューリンが多く共局在している。

B. カルシニューリンと共局在しているアストロサイトの割合を示したもの。それぞれ4症例の大脳皮質から無作為に9ヵ所を拾い，共局在している割合を算出した（単位はコントロール脳を1としたarbitrary unit）。

負荷した際の培地とそのメンブレンを反応させることによって検出する方法である。再現性をもって上昇する因子の中には炎症や細胞接着に関する因子が目立っていたが，その中に，インスリン様成長因子（IGF）に結合し，その生理活性を制御するタンパクであるIGF結合タンパク-3（IGFBP-3）が認められた。後述のように，ADと「IGF抵抗性」は昨今注目されているトピックである。IGFBP-3はその「IGF抵抗性」に深く関与する因子であることから，われわれはIGFBP-3に着目して検証を進めた。実際に，マウス初代培養アストロサイトだけでなくヒトアストロサイトーマ細胞（H4細胞）でも，Aβ刺激によってIGFBP-3の放出が誘導されることを確認した。そのうえで，同じ実験系を用いて免疫抑制剤FK506でカルシニューリンを阻害したところ，IGFBP-3産生が抑制されることが確認された。このことは，マウスのみならずヒトのアストロサイトでも，Aβ刺激によりカルシニューリン経路を介してIGFBP-3の放出が誘導されることを示している。

Ⅳ．ADとIGFBP-3

ADとIGFBP-3との関連は今までもいくつか報告がなされている。その病的意義は明らかではないものの，AD患者の血清IGFBP-3が増加するという報告もあり，バイオマーカーとしても有用である可能性がある[13]。自験例では，ヒト脳サンプルを用いたウエスタンブロットを行ったところ，AD患者脳ではIGFBP-3の発現量が増加していることが確認された。現在までのところ，末梢ではIGFBP-3は肝臓で産生されることが知られているが，脳内のアストロサイトで検出されるIGFBP-3がどこで産生され，どのような機能をもつのかに関しては，決定的なコンセンサスは得られていない。

われわれは，IGFBP-3は中枢内の「アストロサイトで」産生され，「ニューロンに」影響を与えるという仮説のもと脳切片を使って蛍光免疫染色を施行した。図❸にアストロサイトと共存するIGFBP-3を示す。コントロール脳と比較すると，AD患者脳では，アストロサイト内に多くのIGFBP-3が共存していることが見出された。この傾向は，特に老人斑の周囲の活性化したアストロサイト内で多く認められ（data not shown），脳内でAβの刺激によってIGFBP-3の発現が一過性に誘導されている可能性を示す。今後，さらなる病態との関わりについて追求していく必要がある。

Ⅴ．IGF抵抗性とAD

昨今では，生活習慣病がADの危険因子となることが注目されている。なかでも糖尿病はADの大きな危険因子として知られているが，その1つの機序としてインスリン抵抗性が挙げられる。インスリンはニューロンに対して生存シグナルとして働き，そのシグナルの滞りがニューロン障害につながるという仮説である。実際，インスリン抵抗性とADとの関連は数々の報告がなされている[14]。インスリン様成長因子（IGF）は，その名のとおりインスリンと非常に構造が似ており，約50%の構造がインスリンと共通すると言われている[15]。そのような背景もあり，インスリン抵抗性と同様，ADにおける「IGF抵抗性」が病態と関連しているとの報告もなされている[8]。IGFBPはIGFに強い結合力をもつタンパク質であり，IGFBP-3はその中でも最も豊富に存在するサブタイプである。その機能に関しては議論があ

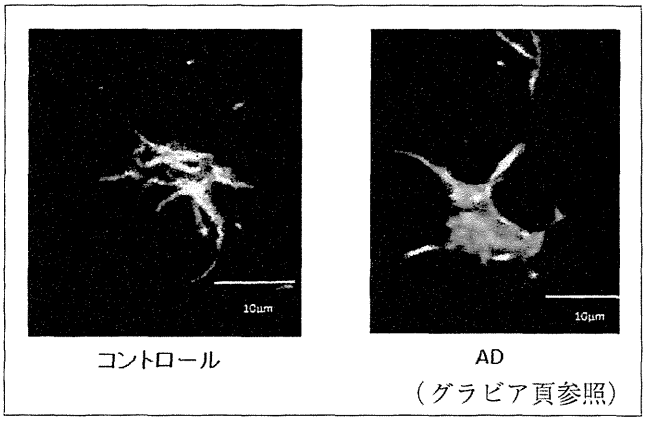

図❸　アストロサイト内のIGFBP-3
緑色に染色された細胞がアストロサイトで，赤色でIGFBP-3が染色されている。コントロールでは，アストロサイト内にIGFBP-3はほとんど認めないのに対して，AD脳では，アストロサイト内にIGFBP-3が非常に多く共局在している様子がわかる。

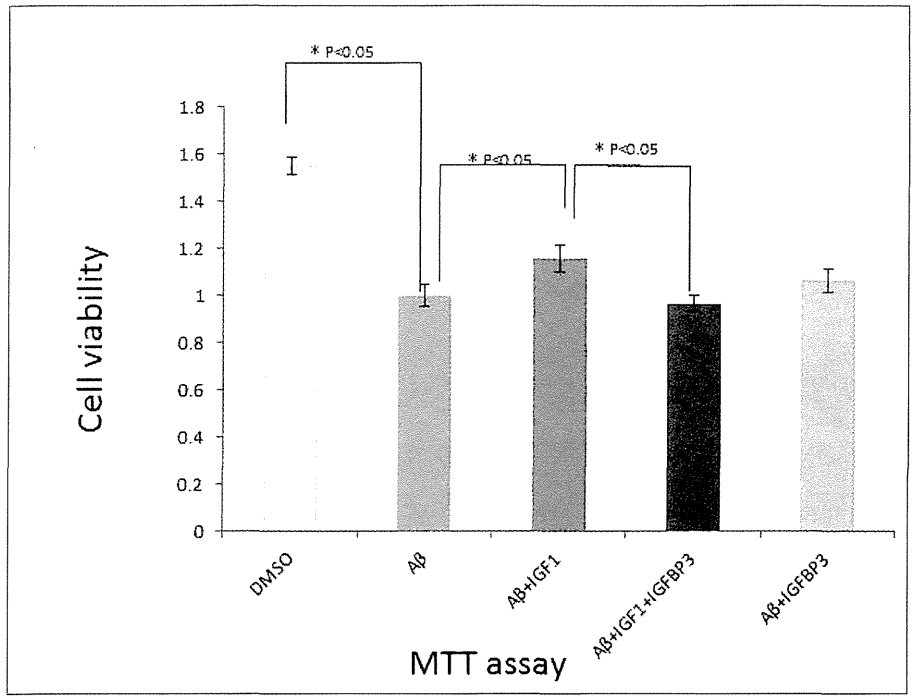

図❹　細胞死に対するIGF-1，IGFBP-3の影響

マウス初代培養ニューロンに，Aβ，IGF-1，IGFBP-3を負荷し，MTTアッセイにより細胞死を検証した。IGF-1はAβによる細胞死を抑制する働きがあるのに対して，IGFBP-3はIGF-1の効果をキャンセルする作用をもっている。

るが，IGFと結合し，目的の組織まで運搬するために必要な因子であると言われている[16]。しかし，その結合の強さゆえ，Aβ負荷によりアストロサイトから放出されるIGFBPが異常に増加した場合，IGFとのバランスが崩れ，生存シグナルであるIGFシグナルの阻害をする，つまりIGF抵抗性に寄与する可能性が考えられる。そこでわれわれは，マウス初代培養ニューロンを用いた細胞死実験を行った。初代培養ニューロンにAβを負荷し，細胞死を促したうえで，IGF，IGFBP-3がどのように影響を与えるかをMTTアッセイで調べてみたところ（図❹），IGFはAβによる細胞死を抑制するのに対して，IGFBP-3存在下ではその作用が阻害されていた。このことから，IGFBP-3はIGFのもつ細胞生存作用を阻害する可能性をもっていることが示された。

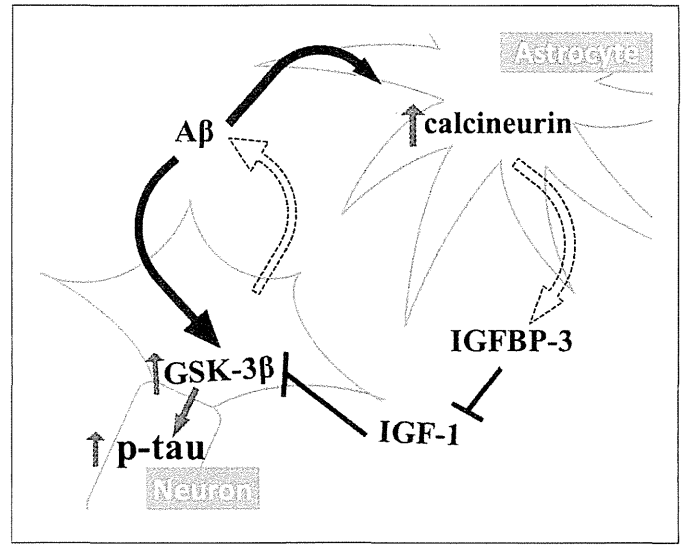

図❺　アストロサイトとニューロンの相互関係

おわりに

ADでは老人斑の主成分であるAβが最初期から蓄積することが知られているが，これまでのモデルマウスの検討からは，Aβのみでは神経細胞死や神経原線維変化が起きないことが指摘されている。こうした神経細胞死につながる経路を考えるうえで，ニューロンにのみ注目しただけでは，どうしても限界があると考えている。実際の脳内環境を少しでも再現しようと思う場合，多くの登場人物との関わりに着目することは非常に大切な

ことである。今回われわれは，アストロサイトとニューロンの相互関係に着目してADの病態生理に新しいアプローチを試みた。神経活動に伴ってニューロンから放出されたAβが，アストロサイトのカルシウム動態を制御し，そのカルシニューリン経路を介して放出されたIGFBP-3が再びニューロンに影響し，細胞死が促されるという流れである（図❺）。われわれのarrayの結果から，アストロサイトから放出が促される因子は他にも数多く存在することが示されており，まだまだ多くの登場人物との関わりのうえで実験を進めるべきではあるが，こうした脳内環境を総合的に捉えることがADの病態生理を紐解く1つの突破口になることを願っている。

参考文献

1) Alzheimer A, et al : Clin Anat 8, 429-431, 1995.
2) Masters CL, et al : Proc Natl Acad Sci USA 82, 4245-4249, 1985.
3) Mandelkow EM, et al : Trends Cell Biol 8, 425-427, 1998.
4) Itagaki S, et al : J Neuroimmunol 24, 173-182, 1989.
5) Ransohoff RM, et al : J Clin Invest 122, 1164-1171, 2012.
6) Green KN, et al : Neuron 59, 190-194, 2008.
7) Khandelwal PJ, et al : J Neuroimmunol 238, 1-11, 2011.
8) Cohen E, et al : Cell 139, 1157-1169, 2009.
9) Talantova M, et al : Proc Natl Acad Sci USA 110, E2518-2527, 2013.
10) Abdul HM, et al : Mol Cell Pharmacol 2, 7-14, 2010.
11) Rusnak F, et al : Physiol Rev 80, 1483-1521, 2000.
12) Malleret G, et al : Cell 104, 675-686, 2001.
13) Johansson P, et al : Psychoneuroendocrinology 38, 1729-1737, 2013.
14) De Felice FG : J Clin Invest 123, 531-539, 2013.
15) Sarfstein R, et al : Endocrinology 154,1672-1679, 2013.
16) Nguyen DV, et al : Growth Horm IGF Res 23, 45-52, 2013.

参考ホームページ

・京都大学医学研究科人間健康科学系専攻木下研究室
http://kinoshita-lab.hs.med.kyoto-u.ac.jp/index.html

渡邉　究
2005年　京都大学医学部卒業
大津赤十字病院神経内科
2006年　京都大学医学部附属病院神経内科
2007年　大津赤十字病院神経内科
2010年　京都大学医学部大学院博士課程（臨床神経学）

BMC Cancer

RESEARCH ARTICLE Open Access

Prognostic prediction of glioblastoma by quantitative assessment of the methylation status of the entire *MGMT* promoter region

Manabu Kanemoto[1,2], Mitsuaki Shirahata[3], Akiyo Nakauma[1], Katsumi Nakanishi[1], Kazuya Taniguchi[1], Yoji Kukita[1], Yoshiki Arakawa[2], Susumu Miyamoto[2] and Kikuya Kato[1*]

Abstract

Background: O6-methylguanine-DNA methyltransferase (*MGMT*) promoter methylation is reported to be a prognostic and predictive factor of alkylating chemotherapy for glioblastoma patients. Methylation specific PCR (MSP) has been most commonly used when the methylation status of *MGMT* is assessed. However, technical obstacles have hampered the implementation of MSP-based diagnostic tests. We quantitatively analyzed the methylation status of the entire *MGMT* promoter region and applied this information for prognostic prediction using sequencing technology.

Methods: Between 1998 and 2012, the genomic DNA of 85 tumor samples from newly diagnosed glioblastoma patients was subjected to bisulfite treatment and subdivided into a training set, consisting of fifty-three samples, and a test set, consisting of thirty-two samples. The training set was analyzed by deep Sanger sequencing with a sequencing coverage of up to 96 clones per sample. This analysis quantitatively revealed the degree of methylation of each cytidine phosphate guanosine (CpG) site. Based on these data, we constructed a prognostic prediction system for glioblastoma patients using a supervised learning method. We then validated this prediction system by deep sequencing with a next-generation sequencer using a test set of 32 samples.

Results: The methylation status of the *MGMT* promoter was correlated with progression-free survival (PFS) in our patient population in the training set. The degree of correlation differed among the CpG sites. Using the data from the top twenty CpG sites, we constructed a prediction system for overall survival (OS) and PFS. The system successfully classified patients into good and poor prognosis groups in both the training set (OS, $p = 0.0381$; PFS, $p = 0.00122$) and the test set (OS, $p = 0.0476$; PFS, $p = 0.0376$). Conventional MSP could not predict the prognosis in either of our sets. (training set: OS; $p = 0.993$ PFS; $p = 0.113$, test set: OS; $p = 0.326$ PFS; $p = 0.342$).

Conclusions: The prognostic ability of our prediction system using sequencing data was better than that of methylation-specific PCR (MSP). Advances in sequencing technologies will make this approach a plausible option for diagnoses based on *MGMT* promotor methylation.

Keywords: Glioma, O6-methylguanine-DNA methyltransferase, Methylation, Bisulfite genome sequencing, Next-generation sequencing

* Correspondence: katou-ki@mc.pref.osaka.jp
[1]Research Institute, Osaka Medical Center for Cancer and Cardiovascular Diseases, 1-3-3 Nakamichi, Higashinari-ku, Osaka, Japan
Full list of author information is available at the end of the article

Background

A glioblastoma (GB) is a malignant brain tumor with a poor prognosis; the median survival time of GB patients is less than 2 years [1]. The current standard of care for GB patients is maximum surgical resection combined with radiation and concomitant adjuvant temozolomide (TMZ) therapy [2]. The long-term results of the EORTC-NCIC CE.3 trial revealed that the 5-year survival of GB patients approaches 10%, despite the largely poor prognosis [3]. Although novel drugs, such as molecular-targeted drugs, have been developed, their survival benefit has not been confirmed, and these molecular targeted drugs are known to carry risks of specific adverse events [4-6]. Accordingly, it is important to identify patients who may respond to conventional chemo-radiation therapy as part of future personalized care. Although nitrosoureas were commonly used for chemotherapy, TMZ is now used for first-line therapy. These drugs are alkylating agents that add an alkyl group to the O6 position of guanine, damaging the genomic DNA of cancer cells. O6-methylguanine-DNA methyltransferase (MGMT) removes alkyl groups from the O6 position of guanine and plays an important role in DNA repair [7-10]. Therefore, *MGMT* expression is associated with resistance to chemotherapeutic alkylating agents. The expression of *MGMT* is controlled by epigenetic gene silencing [11-13]. The methylation of the *MGMT* promoter is associated with sensitivity to alkylating chemotherapy drugs and is recognized as a prognostic factor for GB patients [14-18].

In recent years, TMZ monotherapy has been attempted for elderly GB or low-grade glioma patients, and an association between the treatment response and the *MGMT* methylation status has been examined [19,20]. These studies demonstrated that the methylation status of *MGMT* is a strong predictive factor of TMZ monotherapy outcomes in elderly GB patients, and the clinical utility of the *MGMT* methylation status is increasing [21,22].

Even with this accumulating clinical evidence, the implementation of diagnostic tests examining the methylation status of the *MGMT* promoter has been difficult. PCR-based techniques, such as methylation-specific PCR (MSP) and quantitative MSP, are the most popular methods of assessment [23,24]. These techniques detect methylation sequences by sequence-specific binding of primers, which is an indirect method and only detects a limited number of methylation sites. DNA sequencing (i.e., bisulfite genomic sequencing) provides more direct information on methylation status. In this context, pyrosequencing is considered a good alternative. However, the target methylation sites of pyrosequencing are also limited [25,26]. The *MGMT* promoter region spans more than one thousand base pairs and contains approximately one hundred potential methylation sites. To assess the methylation status of the *MGMT* promoter, it would be preferable to assess information from all methylation sites and select important CpG sites with survival analysis.

In this report, we performed deep sequencing of the *MGMT* promoter region after bisulfite treatment to clarify the global methylation status of the region. Because the methylation status is not uniform in glioma tissue, it is important to characterize the intratumor heterogeneity of *MGMT* promoter methylation. An analysis of survival data assessed the correlation between each CpG site and the malignancy of the glioblastoma. Based on this correlation, we built a classifier to predict the malignancy of GB using deep sequencing with a next-generation sequencer.

Methods

Patient characteristics

We obtained 85 GB specimens from patients who underwent surgical resection at Kyoto University Hospital and related regional hospitals between 1998 and 2012. The majority of the patients were recruited for a phase II clinical trial [27], and their tissues were used for studies on gene expression profiling [28,29]. Histological diagnoses were established by the Kyoto University Pathology Unit according to the criteria established by the World Health Organization. The protocol was approved by the institutional review board of Kyoto University, and written informed consent was obtained from each of the patients. All tumor specimens were immediately snap frozen upon surgical resection and stored at −80°C until use. Tumor specimens containing 20% or more non-tumor tissue or necrotic areas were excluded from further analysis. The preoperative Karnofsky performance status score of each patient was at least 50 for each case. All patients received radiation therapy with and without alkylating chemotherapy postoperatively. The patient characteristics are shown in Table 1. We divided the data matrix into two data sets: one set consisted of 53 patients and was designated as the training set, and the other set contained 32 patients and was designated as the test set.

DNA extraction and bisulfite treatment

Genomic DNA was extracted with the QIAamp DNA Mini Kit (Qiagen) according to the manufacturer's instructions. One nanogram of genomic DNA was subjected to bisulfite treatment using the MethylEasy DNA Bisulfite Modification Kit (Takara) in accordance with the manufacturer's instructions. We determined the quality of bisulfite-treated genomic DNA by real-time PCR of the actin gene as previously described [30]. The outline of the procedure is schematically shown in Additional file 1: Figure S1.

Table 1 Patients' clinical characteristics

Sample		85	
Age		6-88	Median: 60
Gender	Female	36	
	Male	49	
Removal	Biopsy	1	
	Partial	29	
	Subtotal	28	
	Total	20	
	Unknown	8	
Post operative therapy	VAC-feron	57	
	Temozolomide	14	
	Other ACNU regimen	4	
	Radiation alone	7	
	Other	3	
Overall survival (months)		3-96	Median: 12
Progression free survival (months)		1-96	Median: 6

Methylation-specific PCR (MSP)

Conventional MSP was performed as previously described [31]. PCR was performed using AmpliTaq Gold polymerase and the GeneAmp PCR system 9700 (Applied Biosystems). The sequences of the primer pairs were 5′-TTTGTGTTTTGATGTTTGTAGGTTTTTGT-3′ and 5′-AACTCCACACTCTTCCAAAAACAAAACA-3′ for unmethylated *MGMT* (fragment size: 93 bp) and 5′- TTTCGACGTTCGTAGGTTTTCGC -3′ and 5′-GCA CTCTTCCGAAAACGAAACG-3′ for methylated *MGMT* (fragment size: 81 bp). These sequences and the PCR primer sequences used in the further analysis were constructed according to the *MGMT* promoter sequence (http://www.ncbi.nlm.nih.gov/nuccore/X61657.1). After an initial incubation at 95°C for 12 min, PCR amplification was performed with 40 cycles of 95°C for 15 sec, 59°C for 30 sec, and 72°C for 30 sec, followed by a 4-min final extension. The PCR products were electrophoresed on 2% agarose gels and were classified as methylated if a band with the PCR product was visualized using the methylated primer. The experiments were performed twice to confirm the reproducibility of the results. There were no discrepancies between duplicate reactions.

Quantitative bisulfite genome sequencing (qBGS) of the training set

For qBGS, the *MGMT* promoter region was amplified by nested PCR. The sequences of the first-round PCR primers were 5′-TGGTAAATTAAGGTATAGAGTTTT AGG-3′ and 5′-GGTTAGGTGTTAGTGATGTT-3′. The PCR protocol was optimized for bisulfite-treated genomic DNA; each 10-μl reaction mixture of the modified protocol contained 2.5 mM $MgCl_2$, 3% DMSO, 20 ng bisulfite-treated genomic DNA, and 1 μl of AmpliTaq Gold. After an initial incubation at 95°C for 12 min, PCR amplification was performed using 30 cycles of 95°C for 15 sec, 54°C for 30 sec and 72°C for 1 min, followed by a 4-min final extension. A 1-μl aliquot of the first-round PCR product was used as the template of the second-round PCR reaction. The sequences of the second-round PCR primers were 5′-TGGTAAATTAAGGTATAGAGTTTTAGG-3′ and 5′-TT GGATTAGGTTTTTGGGGTT-3′ (fragment size: 662 bp). The genomic position is chr 10: 131,155,100-131,155,761. The second-round PCR was performed using KOD-plus DNA polymerase (TOYOBO) according to the manufacturer's instructions with 1.5 mM $MgSO_4$ and 3% DMSO. After an initial incubation at 95°C for 2 min, PCR amplification was performed with 30 cycles of 94°C for 15 sec, 58°C for 30 sec, and 68°C for 1 min. The PCR products were purified using the MinElute PCR Purification Kit (QIAGEN) and ligated into the pCR-Blunt plasmid using the Zero Blunt PCR Cloning Kit (Invitrogen) and a DNA ligation kit (Takara). MAX Efficiency DH5 Competent Cells (Invitrogen) were used for transformations. A total of 96 colonies of each sample were subjected to bisulfite sequencing using a 3730xl DNA Analyzer (Applied Biosystems). The methylation status was analyzed with QUMA web tools (http://quma.cdb.riken.jp/).

qBGS for the test set

For the test set, we used next-generation sequencing (MiSeq, Illumina) instead of Sanger sequencing. The target sequence was amplified by nested PCR. PCR amplification was performed using 40 cycles of 94°C for 30 sec, 54°C for 30 sec, and 72°C for 45 min, followed by a 4-min final extension. The sequences of the first-round PCR primers were 5′-GGATATGTTGGGATAGTT-3′ and 5′-CCAAAAACCCCAAACCC-3′ [26]. The sequences of the second-round PCR primers were 5′-GGATATGTTGGGATAGTT-3′ and 5′- AAATAAATAA AAATCAAAAC-3′ (fragment size: 216 bp). The annealing temperature was 48°C in the second-round PCR. The PCR product was attached with an adapter for MiSeq plus, consisting of an eight- or six-base index. The pooled PCR library of the test set samples was sequenced by paired-end sequencing with a MiSeq sequencer. Paired-end reads were aligned to a C-to-T converted reference sequence of the *MGMT* promoter region using BWA [32]. We used SAMtools to obtain the per-base coverage (pileup files) and counted non-bisulfite converted sites [33].

Statistical analysis

Statistical analyses were performed using the free statistics software R (http://www.r-project.org/). Overall survival (OS) and progression-free survival (PFS) were defined as the period from surgery to death and from surgery to radiological detection of tumor progression,

respectively. Tumor progression was diagnosed based on the criteria of the Brain Tumor Registry committee (Japan), which includes: a 25% increase in tumor size, the appearance of new lesions, or the obvious deterioration of the patient due to a mass effect or perifocal edema (in Table 1).

Results

Quantitative bisulfite genome sequencing of the training set

Bisulfite sequencing was performed to fully analyze the methylation status of the *MGMT* promoter region. Due to intratumor heterogeneity, the methylation status of individual cells is not identical, even within a single glioma tissue. To clarify this heterogeneity, we performed quantitative bisulfite sequencing and obtained data from 25 to 81 molecules (median, 51) from each sample. This approach is referred to as quantitative bisulfite genome sequencing (qBGS). The 662-bp fragment subjected to qBGS contained 78 CpG sites. One CpG site that is not located within the CpG island of the *MGMT* promoter region was excluded from further analysis. The methylation proportion at each CpG site was calculated as the fraction of clones with a methylated C at that site in all sequenced clones. The methylation status of the *MGMT* promoter region was then described as a data point in a 77-dimensional space constructed from the methylation proportions of the 77 CpG sites. We performed a hierarchical cluster analysis with the Ward method using the raw methylation proportion without any standardization to obtain a general view of the global methylation features of the *MGMT* promoter region. The cases were grouped into four clusters (Figure 1A). These clusters were correlated with the degree of methylation. The column bars below the clustering indicate the MSP results for 53 samples. Typical examples of qBGS results are shown in Figure 2. The samples in cluster 1 were strongly methylated, the samples in cluster 2 were moderately methylated, the samples in cluster 3 were slightly methylated, and the samples in cluster 4 were almost

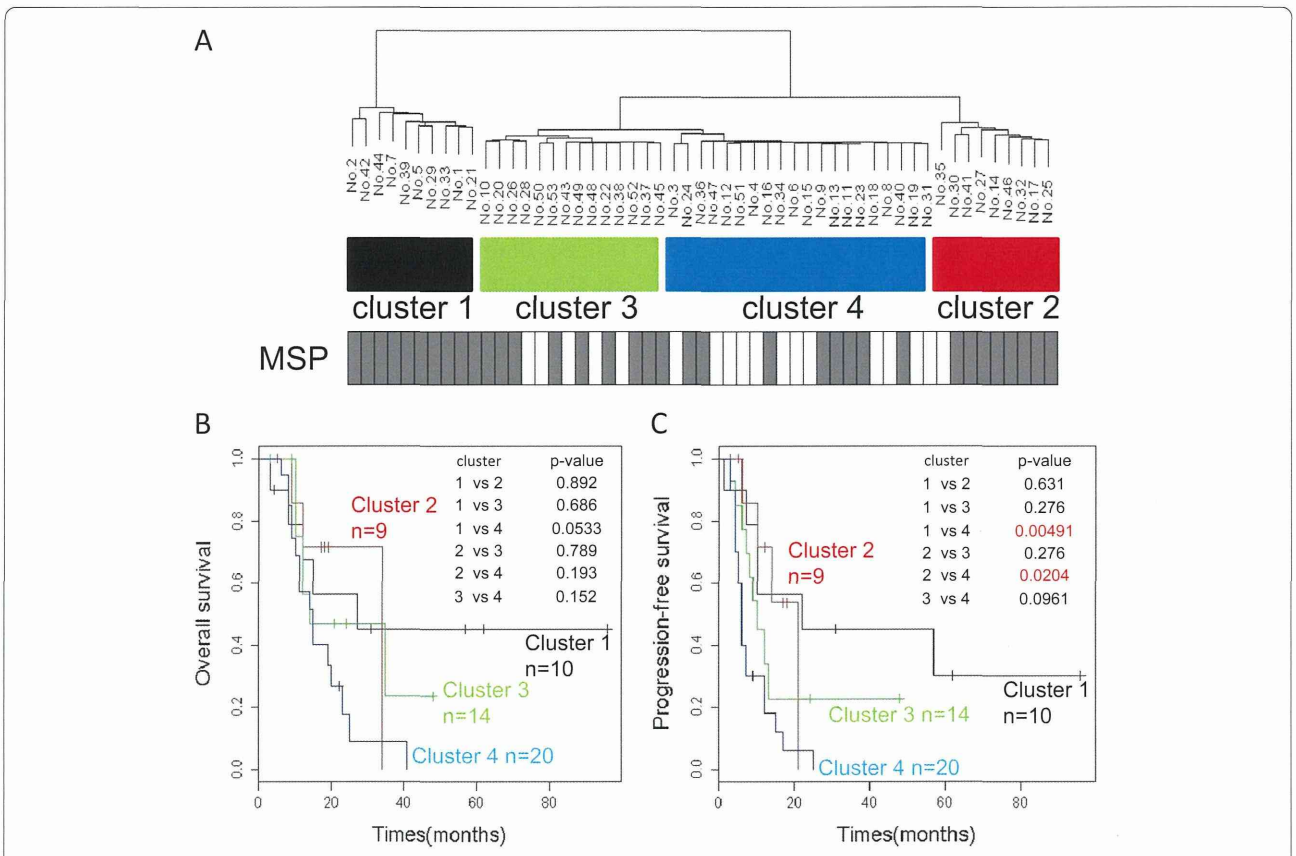

Figure 1 Clustering of the training set and survival analysis. Unsupervised analysis based on the *MGMT* methylation patterns. **(A)** A hierarchical cluster analysis of the methylation of the MGMT promoter in 53 samples. Cluster 1 (Black), strongly methylated samples; cluster 2 (red), moderately methylated; cluster 3 (green), slightly methylated; cluster 4 (blue), mostly unmethylated. The columns below the clustering show the results obtained using MSP. The gray column indicates methylated, and the white column is unmethylated samples. **(B, C)** Survival analysis was performed between all combinations of the four cluster subgroups. For PFS, the analysis showed statistically significant differences between cluster 1 and cluster 4 ($p = 0.00491$) and between cluster 2 and cluster 4 ($p = 0.0204$). For OS, there was no statistically significant difference between any combination of the four clusters, but there was a trend toward a difference between cluster 1 and cluster 4 ($p = 0.0533$).

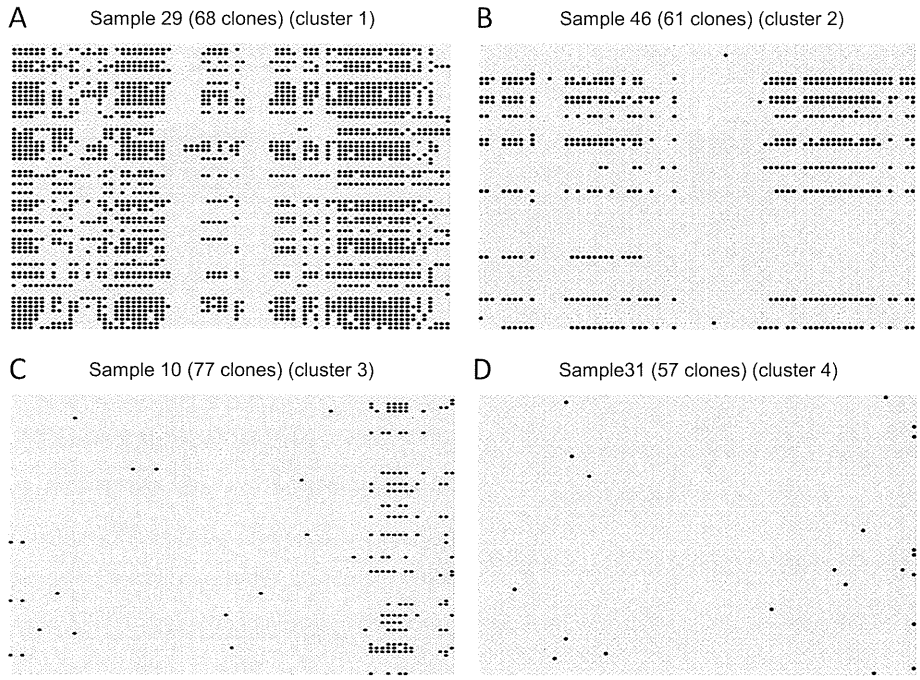

Figure 2 Methylation pattern obtained by qBGS. Methylation pattern observed using qBGS. The black and white circles indicate methylated and unmethylated CpG sites, respectively. Horizontally, 77 CpG sites are aligned. Vertically, the sequencing results of individual clones are aligned. **(A)** Sample 29 from cluster 1 of Figure 1; **(B)** sample 46 from cluster 2; **(C)** sample 10 from cluster 3; and **(D)** sample 31 from cluster 4.

unmethylated. There was a trend toward a prognostic difference for OS between cluster 1 and cluster 4 (p = 0.0533) (Figure 1B). Statistically significant associations with PFS were observed between clusters 1 and 4 (p = 0.00491) and between clusters 2 and 4 (p = 0.0204) (Figure 1C). Several cases that were judged to be methylated (i.e., to have a good prognosis) by MSP belonged to clusters 3 and 4 (Figure 1A). For example, samples 13 and 16 belonged to cluster 4; both showed four months of PFS and were described as poor prognosis [2], but were judged to be methylated and to have a good prognosis by MSP.

To demonstrate an overview of the methylation status of the *MGMT* promoter region, the averages of the methylation proportions of the CpG sites are shown in Figure 3. The promoter sequence may be divided into three segments according to the methylation proportions. The methylation level of the CpG sites in the middle segment, from CpG28 to CpG50, was lower than that of the other segments (Figure 3). This area is located just upstream of the transcription start site. We performed univariate Cox proportional hazard analysis of PFS to identify prognostically important CpG sites using the methylation proportion as a continuous variable. Based on an analysis using the 53 training samples, the log-rank p values of 20 CpG sites were less than 0.05. These 20 selected CpG sites were CpG63 (p = 0.0056), CpG64 (p = 0.0088), CpG77 (p = 0.010), CpG62 (p = 0.012), CpG56 (p = 0.012), CpG68 (p = 0.014), CpG11 (p = 0.023), CpG65 (p = 0.025), CpG66 (p = 0.025), CpG59 (p = 0.027), CpG8 (p = 0.028), CpG60 (p = 0.028), CpG10 (p = 0.030), CpG7 (p = 0.034),CpG5 (p = 0.034), CpG61 (p = 0.035), CpG54 (p = 0.038), CpG9 (p = 0.038), CpG47 (p = 0.047), and CpG67 (p = 0.048). Almost all of the selected sites were located at positions from CpG5 to CpG11 or from CpG54 to CpG68 (black columns in Figure 3). However, only five CpG sites were selected for OS under the same condition: CpG8 (p = 0.039), CpG28 (p = 0.041), CpG56 (p = 0.041), CpG5 (p = 0.044), and CpG45 (p = 0.049) (gray columns in Figure 3). Three CpG sites, CpG5, CpG8, and CpG56, showed a correlation with OS and PFS. All of the results of univariate Cox analysis are supplied in Additional file 2 (PFS) and Additional file 3 (OS). Shah et al. reported a similar comprehensive methylation analysis [34]. Their numbering scheme of CpG sites corresponds to the addition of twenty to our numbering scheme of sites.

Diagnostic system for prognosis prediction using quantitative methylation data

As described above, the prognostic significance of each CpG site is limited, and it would be more effective to combine the information from multiple CpG sites. One approach is an unsupervised analysis, including a cluster analysis, shown above. However, to construct a diagnostic system, supervised learning is more appropriate.

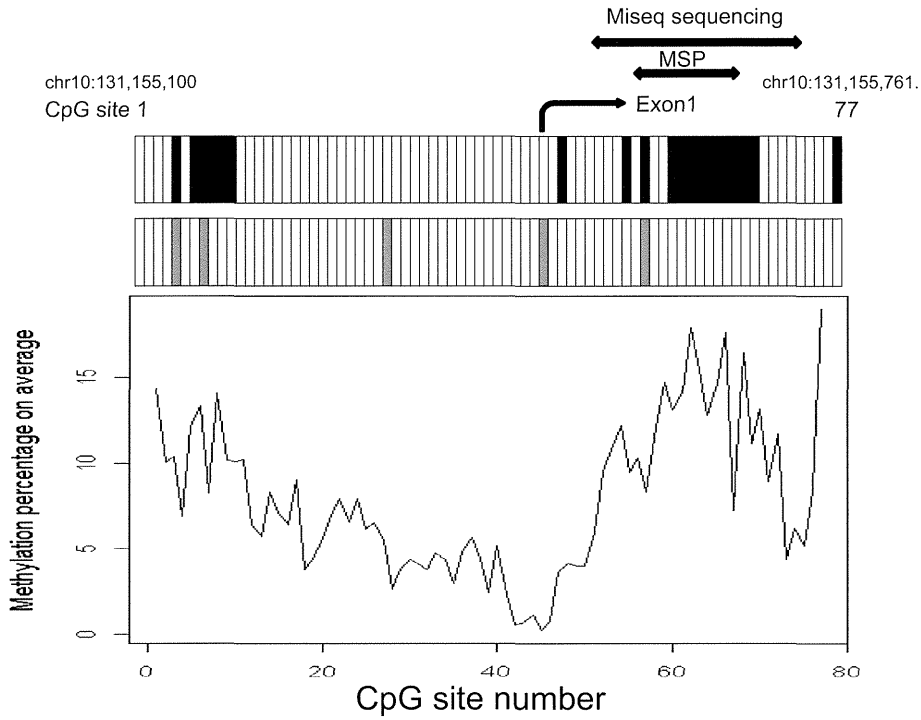

Figure 3 Proportion of methylation status and survival analysis at each CpG site. Average of the methylation percentage of CpG sites. The black and gray columns in the top panel indicate CpG sites with correlations with PFS and OS, respectively, that exceed the threshold ($p < 0.05$).

Here, based on the correlation between OS or PFS and the methylation status of the *MGMT* promoter region, we constructed a diagnostic system to predict the therapeutic outcomes of GB patients based on the methylation proportion of CpG51 - CpG74. Because we intended to use a next-generation sequencer for the validation study, we selected the CpG sites to be examined based on the read length restriction of the sequencer. This diagnostic score was denoted as the M-score (methylation score) and is defined as a weighted sum of the methylation proportion as follows:

$$M\_(methylation)\_score = -\sum_i A_i X_i$$

where 'A_i' is a regression coefficient deduced by univariate Cox analysis of PFS at CpG site i and 'X_i' is the methylation proportion at CpG site i. As described above, a correlation between OS and the methylation status was not clear in our patient population. We therefore used the same M-score calculation formula for OS as well. First, the performance of the M-score diagnostic system was evaluated by leave-one-out-cross-validation (LOOCV) using the 53 training samples. The 53 samples were divided into groups consisting of one and 52 samples, and 'Ai' was calculated by univariate Cox analysis using the data for the remaining 52 samples. The threshold was selected from M-scores of the 52 samples so that the log-rank p value of the Kaplan-Meier analysis for the two divided groups was minimized. In cases of multiple M-scores with the same minimum p value, the median was selected as the threshold. Next, the M-score of the one sample was calculated using parameters deduced from the 52 samples, and the sample was classified into either the good or poor prognosis group using the threshold. This process was repeated until all samples were tested. The LOOCV procedure is schematically shown in Additional file 1: Figure S2. The results of the LOOCV procedure are shown in Figure 4A and B; this approach demonstrated excellent prognostic ability with OS and PFS (OS, $p = 0.0381$; PFS, $p = 0.00122$). Thus, the diagnostic accuracy of our system is better than that of the MSP-based approach (Figure 4C, D) (OS, $p = 0.993$; PFS, $p = 0.113$).

Validation of the diagnostic system using next-generation sequencing

For validation of the test set, the parameters (Ai) were calculated using all 53 samples in the training set, and the threshold was set at 2.2, the average of the thresholds of the 53 LOOCV processes.

For the 32 test set samples, we performed qBGS with a next-generation sequencer, MiSeq, to examine the potential future applications of this approach. We also

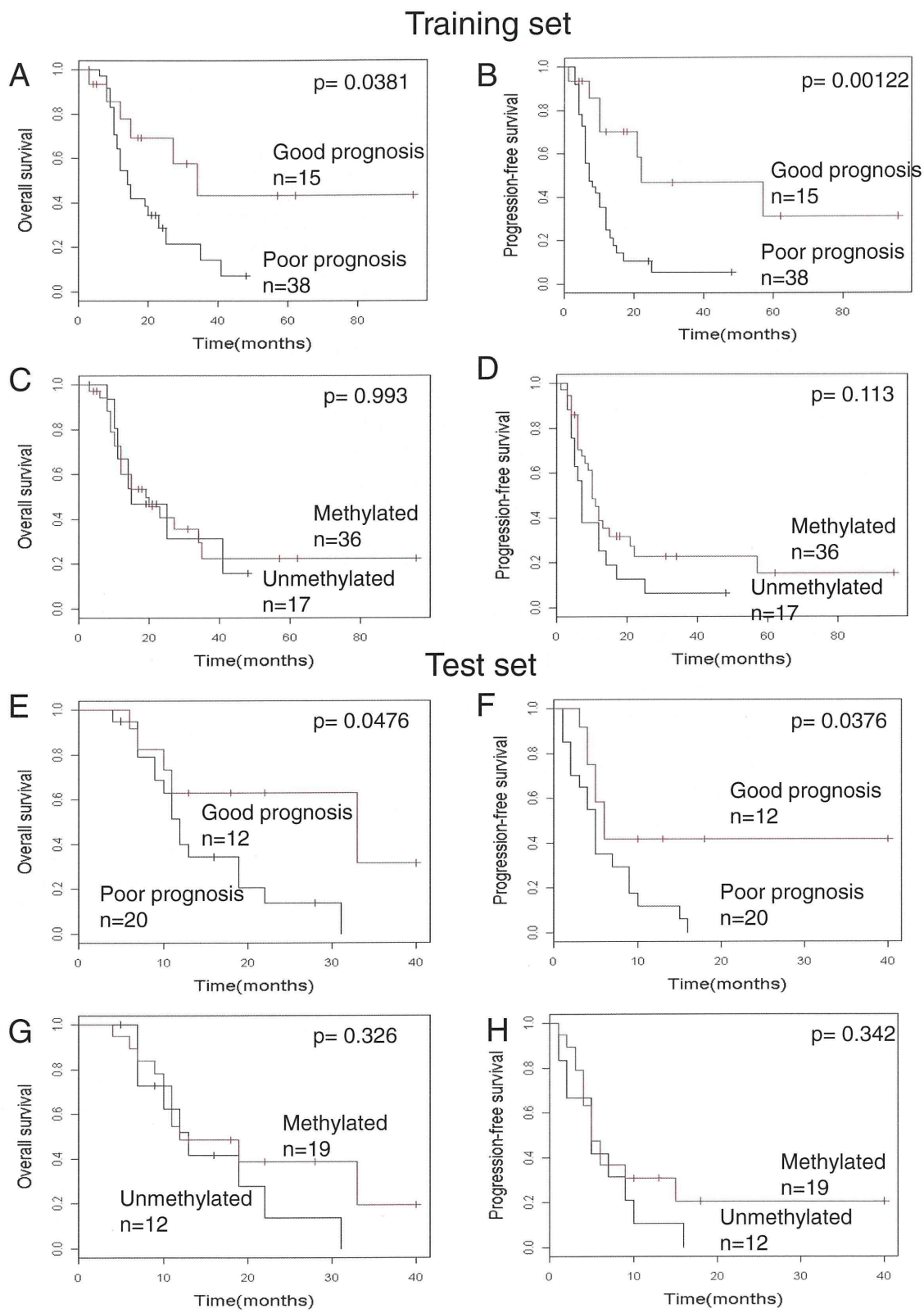

Figure 4 (See legend on next page.)

(See figure on previous page.)
Figure 4 Survival analysis of the training set by M-score and MSP. In each panel, the red line indicates either a good prognosis (M-score) or the methylated (MSP) group. The black line indicates either a poor prognosis (M-score) or the unmethylated (MSP) group. **(A)** training set, M-score, OS. **(B)** training set, M-score, PFS. **(C)** training set, MSP, OS. **(D)** training set, MSP, PFS. **(E)** test set, M-score, OS. **(F)** test set, M-score, PFS. **(G)** test set, MSP, OS. **(H)** test set, MSP, PFS.

performed MSP in all cases except one, due to the loss of genomic DNA. The mean depth of MiSeq sequencing was 80,817 reads. The methylation proportion of each CpG site was obtained, M-scores were calculated, and the test set samples were classified using the threshold listed above. Survival analysis indicated a statistically significant difference between the two groups with respect to PFS ($p = 0.0376$) and OS ($p = 0.0476$) (Figure 4E, F). There was no statistically significant difference between the two groups by classification with MSP (OS, $p = 0.326$; PFS, $p = 0.342$) (Figure 4G, H).

For potential future applications of this technique, we designed PCR primers that amplify the same region from FFPE samples. The method and results are shown in Additional file 4.

Multivariate Cox regression analysis

We performed Cox regression analysis to evaluate clinical parameters, such as age (above or below 60), gender, the extent of resection, post-operative chemotherapy (VAC-feron or TMZ), and the methylation status by the M-score sequencing method as predictors of OS and PFS in the GB patients in the test set. The variables with a p value < 0.2 were analyzed with a backward stepwise Multivariate Cox proportional hazard model. For OS, the best predictor was the M-score ($p = 0.0585$) (Hazard Ratio, 0.3558), and the next best prognostic factor was the extent of surgical resection ($p = 0.0739$) (Hazard Ratio, 0.5996). The M-score was found to be the best predictor of PFS ($p = 0.0247$; Hazard Ratio, 0.334).

Discussion

In this report, we characterized the methylation status of the entire *MGMT* promoter region using deep sequencing. The methylation status of each CpG site was quantitatively evaluated by sequencing multiple clones. Based on these results, we constructed a prognosis predictor that incorporates the methylation status of multiple CpG sites using supervised learning. The construction of a classifier using supervised learning is popular in the field of gene expression profiling, and we demonstrated here that the same approach is effective for the prediction of methylation status.

In our patient population, the correlation of the methylation status with OS was less clear than that with PFS. This is most likely due to variation of the therapy used after the first line therapy. The majority of our patients received repeated surgical resections, second line chemotherapy or additional radiotherapy. For multivariate analysis, age was not a prognosis factor, unlike in the past reports. We also performed surgical medical treatment with methylation-positive elderly patients. In particular, repeated surgery was likely to prolong the survival time of the glioblastoma patients with a poor prognosis.

MSP is the most widely used assay for methylation. However, MSP can only detect the CpG sites in the primer region; the methylation status of other CpG sites has no effect on the amplification. In a prior study, only 12.5% of the results obtained from two MSP experiments matched when the forward and reverse primers were different [35]. In addition, there is no established method to confirm the quality of bisulfite-converted genomic DNA. We assessed the quality using the Ct value of actin in real-time PCR. Approximately 64% of our glioma samples were methylation-positive with MSP. The positive rate was higher than that in other studies with some exceptions [36,37]. We excluded samples damaged by bisulfite treatment in the actin-based confirmation system, and this process may have increased the positive rate. This discrepancy in MSP results, which is most likely a false positive, might be influenced by the T genotype of the *MGMT* C > T (rs16906252) enhancer single-nucleotide polymorphism (SNP), which was reported by McDonald et al. [38] to interact with MGMT promotor methylation. Vlassenbroeck et al. also evaluated the results of qMSP based on the copy number of actin using real-time PCR [39]. It is often difficult to set a threshold for agarose gel patterns of MSP. This problem has been overcome by quantitative MSP [40,41]. Quantitative MSP was applied in two recent phase 3 trials of glioma [21,22]. However, the problem of limited coverage of CpG sites by MSP remains in need of technical improvements.

As discussed above, bisulfite sequencing can cover all CpG sites. In this context, pyrosequencing is considered to cover more CpG sites than MSP [26]. The methylation proportions can be semi-quantitatively deduced from the peak height of each incorporated nucleotide. The main disadvantage of pyrosequencing is its short read length [25,26]. qBGS using Sanger sequencing is not subject to this limitation, and its moderate read depth provides more accurate quantitative information. Because deep sequencing with the Sanger method is laborious, the use of next-generation sequencing may make this approach more comparable to pyrosequencing.

The major shortcoming of qBGS and pyrosequencing is the absence of a consensus regarding the data handling of multidimensional quantitative data. Dunn et al. and Motomura et al. used the average of the methylation proportion of multiple CpG sites (CpG51 - CpG62, Dunn et al.; CpG2 - CpG16, Motomura et al.) [42,43]. Karayan-Tapon et al. used the methylation proportion of five CpG sites (CpG 53–57) and grouped patients using the median value of the methylation proportion as the threshold [25]. We developed the M-score diagnostic system using the analysis method of gene expression profiling and calculated the optimized threshold by LOOCV. The M-score is the weighted sum of the methylation proportions of multiple CpG sites, which maximizes the correlation with the survival time. Our approach is more advanced than a simple summation of the population of methylated sites, and adding data from a larger patient population will improve the performance of the predictor. Bady et al. examined the quantitative value of 18 CpG sites in the *MGMT* promoter area using the Infinium methylation BeadChip and revealed two distinct CpG sites (CpG10 and CpG68). They converted multidimensional data to one methylation probability score using the inverse logit function. The classifier was validated with an external data set [44]. Both studies indicate a new direction for *MGMT* methylation assays based on evaluation of multiple CpG sites.

Shah et al. also quantitatively evaluated the methylation of the *MGMT* promoter [34]. Although the number of sequenced clones in that study was far less than that of our study (median of 10 clones), their results were similar to our results; the CpG sites located downstream of the transcription start site were often correlated with PFS. This prior study indicates that our observations are likely to be universal, and suggests that our prognosis predictor may be applicable to other patient populations.

The identification of biomarkers of gliomas has been an active area of research in recent years. It is well known that *IDH* mutations are a strong prognostic factor [45]. *IDH* mutations are associated with a hypermethylation phenotype [46], suggesting that the methylation of the *MGMT* promoter is one part of a genome-wide methylation profile [47]. Based on qBGS analysis, we identified different extents of methylation of CpG sites in the *MGMT* promoter region.

Recently, the methylation status of *MGMT* has become a focal point in the management of elderly GB patients. Two *MGMT* methylation analyses using samples from large phase 3 trials with elderly GB patients demonstrated that TMZ monotherapy was superior to conventional radiation therapy for the management of *MGMT*-methylated GB patients. Conversely, TMZ monotherapy was inferior to radiation therapy in GB cases with unmethylated *MGMT* [21,22]. These results indicate that the *MGMT* methylation status is a strong predictive factor for the efficacy of TMZ monotherapy in elderly GB patients and that evaluating *MGMT* methylation status is necessary for the management of these patients. The relationship between the efficacy of TMZ monotherapy and qBGS-based methylation analysis of the *MGMT* promoter in elderly GB merits further investigation.

In addition to its application for elderly patients, TMZ monotherapy has been utilized for low-grade glioma patients [20,48]. In this group, the co-deletion of 1p19q and *IDH* mutations were molecular prognostic factors. Given the findings in elderly GB patients, the methylation status of the *MGMT* promoter may also predict the outcomes of low-grade glioma patients treated by TMZ monotherapy. Because the *MGMT* promoter in normal tissue is generally unmethylated, methylated *MGMT* cases are susceptible to contamination by normal tissue. An advantage of qBGS is that it is easy to observe the state of contamination. qBGS also revealed intratumoral heterogeneity in the methylation of the *MGMT* promoter, which should be considered when using other methylation assays. Although qBGS is complicated and time-consuming, it is an important process for evaluating the methylation features of the *MGMT* promoter.

Conclusions

We constructed a novel diagnostic system to predict the prognosis of glioblastoma patients using information regarding the methylation status of the entire *MGMT* promoter region. A precise assessment of the methylation status of the *MGMT* promoter may improve the prediction of disease progression and assist in the choice of TMZ treatment.

Additional files

Additional file 1: Figure S1. Algorithm of quality assessment of bisulfite-treated genomic DNA. **Figure S2.** Schematic representation of leave-one-out cross-validation.

Additional file 2: Table S1. Table of regression coefficients of CpG sites based on PFS.

Additional file 3: Table S2. Table of regression coefficients of CpG sites based on OS.

Additional file 4: Agarose gel image of PCR product using FFPE genomic DNA.

Abbreviations

MGMT: O6-methylguanine-DNA methyltransferase; MSP: Methylation specific PCR, CpG, cytidine phosphate guanosine; PFS: Progression-free survival; OS: Overall survival; GB: Glioblastoma; TMZ: Temozolomide; qBGS: Quantitative bisulfite genome sequencing; DMSO: Dimethyl sulfoxide.

Competing interests

The authors declare that they have no competing interests.

Authors' contributions
MK, AN, KN and KT performed the experiments in this study. MS, YK, YA, SM and KK supervised the research. MK and KK wrote this manuscript. All authors approved the final manuscript.

Author details
[1]Research Institute, Osaka Medical Center for Cancer and Cardiovascular Diseases, 1-3-3 Nakamichi, Higashinari-ku, Osaka, Japan. [2]Department of Neurosurgery, Kyoto University Graduate School of Medicine, 54 Kawahara-cho, Shogoin, Sakyo-ku, Kyoto-shi, Kyoto 606-8507, Japan. [3]Department of Neuro-Oncology/Neurosurgery, Saitama Medical University International Medical Center, 1397-1 Yamane, Hidaka, Saitama 350-1298, Japan.

Received: 4 March 2014 Accepted: 27 August 2014
Published: 30 August 2014

References

1. Anderson E, Grant R, Lewis SC, Whittle IR: **Randomized Phase III controlled trials of therapy in malignant glioma: where are we after 40 years?** *Br J Neurosurg* 2008, **22**(3):339–349.
2. Stupp R, Mason WP, van den Bent MJ, Weller M, Fisher B, Taphoorn MJ, Belanger K, Brandes AA, Marosi C, Bogdahn U, Curschmann J, Janzer RC, Ludwin SK, Gorlia T, Allgeier A, Lacombe D, Cairncross JG, Eisenhauer E, Mirimanoff RO: **Radiotherapy plus concomitant and adjuvant temozolomide for glioblastoma.** *N Engl J Med* 2005, **352**(10):987–996.
3. Stupp R, Hegi ME, Mason WP, van den Bent MJ, Taphoorn MJ, Janzer RC, Ludwin SK, Allgeier A, Fisher B, Belanger K, Hau P, Brandes AA, Gijtenbeek J, Marosi C, Vecht CJ, Mokhtari K, Wesseling P, Villa S, Eisenhauer E, Gorlia T, Weller M, Lacombe D, Cairncross JG, Mirimanoff RO: **Effects of radiotherapy with concomitant and adjuvant temozolomide versus radiotherapy alone on survival in glioblastoma in a randomised phase III study: 5-year analysis of the EORTC-NCIC trial.** *Lancet Oncol* 2009, **10**(5):459–466.
4. Chinot OL, Wick W, Saran F, Mason WP, Henriksson R, Nishikawa R, Zeaiter AH, Moore N, Das A, Cloughesy TF: **AVAglio: a phase III trial of bevacizumab added to standard radiotherapy and temozolomide in patients with newly diagnosed glioblastoma.** *J Clin Oncol* 2011, **29**(suppl):abstr TPS136.
5. Friedman HS, Prados MD, Wen PY, Mikkelsen T, Schiff D, Abrey LE, Yung WK, Paleologos N, Nicholas MK, Jensen R, Vredenburgh J, Huang J, Zheng M, Cloughesy T: **Bevacizumab alone and in combination with irinotecan in recurrent glioblastoma.** *J Clin Oncol* 2009, **27**(28):4733–4740.
6. Gilbert MR, Dignam J, Won M, Blumenthal DT, Vogelbaum MA, Aldape KD, Colman H, Chakravarti A, Jeraj R, Armstrong TS, Wefel JS, Brown PD, Jaeckle KA, Schiff D, Atkins JN, Brachman D, Werner-Wasik M, Komaki R, Sulman EP, Mehta MP: **RTOG 0825: Phase III double-blind placebo-controlled trial evaluating bevacizumab (Bev) in patients (Pts) with newly diagnosed glioblastoma (GBM).** *J Clin Oncol* 2013, **31**(supp):abstr 1.
7. Drablos F, Feyzi E, Aas PA, Vaagbo CB, Kavli B, Bratlie MS, Pena-Diaz J, Otterlei M, Slupphaug G, Krokan HE: **Alkylation damage in DNA and RNA–repair mechanisms and medical significance.** *DNA Repair (Amst)* 2004, **3**(11):1389–1407.
8. Gerson SL: **MGMT: its role in cancer aetiology and cancer therapeutics.** *Nat Rev Cancer* 2004, **4**(4):296–307.
9. Kaina B, Christmann M, Naumann S, Roos WP: **MGMT: key node in the battle against genotoxicity, carcinogenicity and apoptosis induced by alkylating agents.** *DNA Repair (Amst)* 2007, **6**(8):1079–1099.
10. Nagarajan RP, Costello JF: **Epigenetic mechanisms in glioblastoma multiforme.** *Semin Cancer Biol* 2009, **19**(3):188–197.
11. Everhard S, Tost J, El Abdalaoui H, Criniere E, Busato F, Marie Y, Gut IG, Sanson M, Mokhtari K, Laigle-Donadey F, Hoang-Xuan K, Delattre JY, Thillet J: **Identification of regions correlating MGMT promoter methylation and gene expression in glioblastomas.** *Neuro Oncol* 2009, **11**(4):348–356.
12. Gerson SL: **Clinical relevance of MGMT in the treatment of cancer.** *J Clin Oncol* 2002, **20**(9):2388–2399.
13. Verbeek B, Southgate TD, Gilham DE, Margison GP: **O6-Methylguanine-DNA methyltransferase inactivation and chemotherapy.** *Br Med Bull* 2008, **85**:17–33.
14. Esteller M, Garcia-Foncillas J, Andion E, Goodman SN, Hidalgo OF, Vanaclocha V, Baylin SB, Herman JG: **Inactivation of the DNA-repair gene MGMT and the clinical response of gliomas to alkylating agents.** *N Engl J Med* 2000, **343**(19):1350–1354.
15. Gorlia T, van den Bent MJ, Hegi ME, Mirimanoff RO, Weller M, Cairncross JG, Eisenhauer E, Belanger K, Brandes AA, Allgeier A, Lacombe D, Stupp R: **Nomograms for predicting survival of patients with newly diagnosed glioblastoma: prognostic factor analysis of EORTC and NCIC trial 26981-22981/CE.3.** *Lancet Oncol* 2008, **9**(1):29–38.
16. Hegi ME, Diserens AC, Godard S, Dietrich PY, Regli L, Ostermann S, Otten P, Van Melle G, de Tribolet N, Stupp R: **Clinical trial substantiates the predictive value of O-6-methylguanine-DNA methyltransferase promoter methylation in glioblastoma patients treated with temozolomide.** *Clin Cancer Res* 2004, **10**(6):1871–1874.
17. Hegi ME, Diserens AC, Gorlia T, Hamou MF, de Tribolet N, Weller M, Kros JM, Hainfellner JA, Mason W, Mariani L, Bromberg JE, Hau P, Mirimanoff RO, Cairncross JG, Janzer RC, Stupp R: **MGMT gene silencing and benefit from temozolomide in glioblastoma.** *N Engl J Med* 2005, **352**(10):997–1003.
18. Hegi ME, Liu L, Herman JG, Stupp R, Wick W, Weller M, Mehta MP, Gilbert MR: **Correlation of O6-methylguanine methyltransferase (MGMT) promoter methylation with clinical outcomes in glioblastoma and clinical strategies to modulate MGMT activity.** *J Clin Oncol* 2008, **26**(25):4189–4199.
19. Gallego Perez-Larraya J, Ducray F, Chinot O, Catry-Thomas I, Taillandier L, Guillamo JS, Campello C, Monjour A, Cartalat-Carel S, Barrie M, Huchet A, Beauchesne P, Matta M, Mokhtari K, Tanguy ML, Honnorat J, Delattre JY: **Temozolomide in elderly patients with newly diagnosed glioblastoma and poor performance status: an ANOCEF phase II trial.** *J Clin Oncol* 2011, **29**(22):3050–3055.
20. Taal W, Dubbink HJ, Zonnenberg CB, Zonnenberg BA, Postma TJ, Gijtenbeek JM, Boogerd W, Groenendijk FH, Kros JM, Kouwenhoven MC, van Marion R, van Heuvel I, van der Holt B, Bromberg JE, Sillevis Smitt PA, Dinjens WN, van den Bent MJ: **First-line temozolomide chemotherapy in progressive low-grade astrocytomas after radiotherapy: molecular characteristics in relation to response.** *Neuro Oncol* 2011, **13**(2):235–241.
21. Malmstrom A, Gronberg BH, Marosi C, Stupp R, Frappaz D, Schultz H, Abacioglu U, Tavelin B, Lhermitte B, Hegi ME, Rosell J, Henriksson R: **Temozolomide versus standard 6-week radiotherapy versus hypofractionated radiotherapy in patients older than 60 years with glioblastoma: the Nordic randomised, phase 3 trial.** *Lancet Oncol* 2012, **13**(9):916–926.
22. Wick W, Platten M, Meisner C, Felsberg J, Tabatabai G, Simon M, Nikkhah G, Papsdorf K, Steinbach JP, Sabel M, Combs SE, Vesper J, Braun C, Meixensberger J, Ketter R, Mayer-Steinacker R, Reifenberger G, Weller M: **Temozolomide chemotherapy alone versus radiotherapy alone for malignant astrocytoma in the elderly: the NOA-08 randomised, phase 3 trial.** *Lancet Oncol* 2012, **13**(7):707–715.
23. Parkinson JF, Wheeler HR, Clarkson A, McKenzie CA, Biggs MT, Little NS, Cook RJ, Messina M, Robinson BG, McDonald KL: **Variation of O(6)-methylguanine-DNA methyltransferase (MGMT) promoter methylation in serial samples in glioblastoma.** *J Neurooncol* 2008, **87**(1):71–78.
24. Rand K, Qu W, Ho T, Clark SJ, Molloy P: **Conversion-specific detection of DNA methylation using real-time polymerase chain reaction (ConLight-MSP) to avoid false positives.** *Methods* 2002, **27**(2):114–120.
25. Karayan-Tapon L, Quillien V, Guilhot J, Wager M, Fromont G, Saikali S, Etcheverry A, Hamlat A, Loussouarn D, Campion L, Campone M, Vallette FM, Gratas-Rabbia-Re C: **Prognostic value of O6-methylguanine-DNA methyltransferase status in glioblastoma patients, assessed by five different methods.** *J Neurooncol* 2010, **97**(3):311–322.
26. Mikeska T, Bock C, El-Maarri O, Hubner A, Ehrentraut D, Schramm J, Felsberg J, Kahl P, Buttner R, Pietsch T, Waha A: **Optimization of quantitative MGMT promoter methylation analysis using pyrosequencing and combined bisulfite restriction analysis.** *J Mol Diagn* 2007, **9**(3):368–381.
27. Aoki T, Takahashi JA, Ueba T, Oya N, Hiraoka M, Matsui K, Fukui T, Nakashima Y, Ishikawa M, Hashimoto N: **Phase II study of nimustine, carboplatin, vincristine, and interferon-beta with radiotherapy for glioblastoma multiforme: experience of the Kyoto Neuro-Oncology Group.** *J Neurosurg* 2006, **105**(3):385–391.
28. Shirahata M, Iwao-Koizumi K, Saito S, Ueno N, Oda M, Hashimoto N, Takahashi JA, Kato K: **Gene expression-based molecular diagnostic system for malignant gliomas is superior to histological diagnosis.** *Clin Cancer Res* 2007, **13**(24):7341–7356.
29. Shirahata M, Oba S, Iwao-Koizumi K, Saito S, Ueno N, Oda M, Hashimoto N, Ishii S, Takahashi JA, Kato K: **Using gene expression profiling to identify a prognostic molecular spectrum in gliomas.** *Cancer Sci* 2009, **100**(1):165–172.

30. Reesink-Peters N, Wisman GB, Jeronimo C, Tokumaru CY, Cohen Y, Dong SM, Klip HG, Buikema HJ, Suurmeijer AJ, Hollema H, Boezen HM, Sidransky D, van der Zee AG: **Detecting cervical cancer by quantitative promoter hypermethylation assay on cervical scrapings: a feasibility study.** *Mol Cancer Res* 2004, **2**(5):289–295.
31. Esteller M, Hamilton SR, Burger PC, Baylin SB, Herman JG: **Inactivation of the DNA repair gene O6-methylguanine-DNA methyltransferase by promoter hypermethylation is a common event in primary human neoplasia.** *Cancer Res* 1999, **59**(4):793–797.
32. Li H, Durbin R: **Fast and accurate short read alignment with Burrows-Wheeler transform.** *Bioinformatics* 2009, **25**(14):1754–1760.
33. Li H, Handsaker B, Wysoker A, Fennell T, Ruan J, Homer N, Marth G, Abecasis G, Durbin R: **The Sequence Alignment/Map format and SAMtools.** *Bioinformatics* 2009, **25**(16):2078–2079.
34. Shah N, Lin B, Sibenaller Z, Ryken T, Lee H, Yoon JG, Rostad S, Foltz G: **Comprehensive analysis of MGMT promoter methylation: correlation with MGMT expression and clinical response in GBM.** *PLoS One* 2011, **6**(1):e16146.
35. van Nifterik KA, van den Berg J, van der Meide WF, Ameziane N, Wedekind LE, Steenbergen RD, Leenstra S, Lafleur MV, Slotman BJ, Stalpers LJ, Sminia P: **Absence of the MGMT protein as well as methylation of the MGMT promoter predict the sensitivity for temozolomide.** *Br J Cancer* 2010, **103**(1):29–35.
36. Gerstner ER, Yip S, Wang DL, Louis DN, Iafrate AJ, Batchelor TT: **Mgmt methylation is a prognostic biomarker in elderly patients with newly diagnosed glioblastoma.** *Neurology* 2009, **73**(18):1509–1510.
37. Reifenberger G, Hentschel B, Felsberg J, Schackert G, Simon M, Schnell O, Westphal M, Wick W, Pietsch T, Loeffler M, Weller M: **Predictive impact of MGMT promoter methylation in glioblastoma of the elderly.** *Int J Cancer* 2012, **131**(6):1342–1350.
38. McDonald KL, Rapkins RW, Olivier J, Zhao L, Nozue K, Lu D, Tiwari S, Kuroiwa-Trzmielina J, Brewer J, Wheeler HR, Hitchins MP: **The T genotype of the MGMT C > T (rs16906252) enhancer single-nucleotide polymorphism (SNP) is associated with promoter methylation and longer survival in glioblastoma patients.** *Eur J Cancer* 2013, **49**(2):360–368.
39. Vlassenbroeck I, Califice S, Diserens AC, Migliavacca E, Straub J, Di Stefano I, Moreau F, Hamou MF, Renard I, Delorenzi M, Flamion B, DiGuiseppi J, Bierau K, Hegi ME: **Validation of real-time methylation-specific PCR to determine O6-methylguanine-DNA methyltransferase gene promoter methylation in glioma.** *J Mol Diagn* 2008, **10**(4):332–337.
40. Hattermann K, Mehdorn HM, Mentlein R, Schultka S, Held-Feindt J: **A methylation-specific and SYBR-green-based quantitative polymerase chain reaction technique for O6-methylguanine DNA methyltransferase promoter methylation analysis.** *Anal Biochem* 2008, **377**(1):62–71.
41. Metellus P, Coulibaly B, Nanni I, Fina F, Eudes N, Giorgi R, Barrie M, Chinot O, Fuentes S, Dufour H, Ouafik L, Figarella-Branger D: **Prognostic impact of O6-methylguanine-DNA methyltransferase silencing in patients with recurrent glioblastoma multiforme who undergo surgery and carmustine wafer implantation: a prospective patient cohort.** *Cancer* 2009, **115**(20):4783–4794.
42. Dunn J, Baborie A, Alam F, Joyce K, Moxham M, Sibson R, Crooks D, Husband D, Shenoy A, Brodbelt A, Wong H, Liloglou T, Haylock B, Walker C: **Extent of MGMT promoter methylation correlates with outcome in glioblastomas given temozolomide and radiotherapy.** *Br J Cancer* 2009, **101**(1):124–131.
43. Motomura K, Natsume A, Kishida Y, Higashi H, Kondo Y, Nakasu Y, Abe T, Namba H, Wakai K, Wakabayashi T: **Benefits of interferon-beta and temozolomide combination therapy for newly diagnosed primary glioblastoma with the unmethylated MGMT promoter: A multicenter study.** *Cancer* 2011, **117**(8):1721–1730.
44. Bady P, Sciuscio D, Diserens AC, Bloch J, van den Bent MJ, Marosi C, Dietrich PY, Weller M, Mariani L, Heppner FL, McDonald DR, Lacombe D, Stupp R, Delorenzi M, Hegi ME: **MGMT methylation analysis of glioblastoma on the Infinium methylation BeadChip identifies two distinct CpG regions associated with gene silencing and outcome, yielding a prediction model for comparisons across datasets, tumor grades, and CIMP-status.** *Acta Neuropathol* 2012, **124**(4):547–560.
45. Yan H, Parsons DW, Jin G, McLendon R, Rasheed BA, Yuan W, Kos I, Batinic-Haberle I, Jones S, Riggins GJ, Friedman H, Friedman A, Reardon D, Herndon J, Kinzler KW, Velculescu VE, Vogelstein B, Bigner DD: **IDH1 and IDH2 mutations in gliomas.** *N Engl J Med* 2009, **360**(8):765–773.
46. Noushmehr H, Weisenberger DJ, Diefes K, Phillips HS, Pujara K, Berman BP, Pan F, Pelloski CE, Sulman EP, Bhat KP, Verhaak RG, Hoadley KA, Hayes DN, Perou CM, Schmidt HK, Ding L, Wilson RK, Van Den Berg D, Shen H, Bengtsson H, Neuvial P, Cope LM, Buckley J, Herman JG, Baylin SB, Laird PW, Aldape K: **Identification of a CpG island methylator phenotype that defines a distinct subgroup of glioma.** *Cancer Cell* 2010, **17**(5):510–522.
47. van den Bent MJ, Gravendeel LA, Gorlia T, Kros JM, Lapre L, Wesseling P, Teepen JL, Idbaih A, Sanson M, Smitt PA, French PJ: **A hypermethylated phenotype is a better predictor of survival than MGMT methylation in anaplastic oligodendroglial brain tumors: a report from EORTC study 26951.** *Clin Cancer Res* 2011, **17**(22):7148–7155.
48. Hoang-Xuan K, Capelle L, Kujas M, Taillibert S, Duffau H, Lejeune J, Polivka M, Criniere E, Marie Y, Mokhtari K, Carpentier AF, Laigle F, Simon JM, Cornu P, Broet P, Sanson M, Delattre JY: **Temozolomide as initial treatment for adults with low-grade oligodendrogliomas or oligoastrocytomas and correlation with chromosome 1p deletions.** *J Clin Oncol* 2004, **22**(15):3133–3138.

doi:10.1186/1471-2407-14-641
Cite this article as: Kanemoto *et al.*: Prognostic prediction of glioblastoma by quantitative assessment of the methylation status of the entire *MGMT* promoter region. *BMC Cancer* 2014 **14**:641.

NeuroImage: Clinical 5 (2014) 396–407

Contents lists available at ScienceDirect

NeuroImage: Clinical

journal homepage: www.elsevier.com/locate/ynicl

Voxel-based clustered imaging by multiparameter diffusion tensor images for glioma grading

Rika Inano[a,b], Naoya Oishi[b,*], Takeharu Kunieda[a], Yoshiki Arakawa[a], Yukihiro Yamao[a,b], Sumiya Shibata[a,b], Takayuki Kikuchi[a], Hidenao Fukuyama[b], Susumu Miyamoto[a]

[a]Department of Neurosurgery, Kyoto University Graduate School of Medicine, Kyoto, Japan
[b]Human Brain Research Center, Kyoto University Graduate School of Medicine, Kyoto, Japan

ARTICLE INFO

Article history:
Received 2 June 2014
Received in revised form 15 July 2014
Accepted 5 August 2014
Available online 7 August 2014

Keywords:
Glioma grading
Diffusion tensor imaging
Voxel-based clustering
Self-organizing map
K-means
Support vector machine

ABSTRACT

Gliomas are the most common intra-axial primary brain tumour; therefore, predicting glioma grade would influence therapeutic strategies. Although several methods based on single or multiple parameters from diagnostic images exist, a definitive method for pre-operatively determining glioma grade remains unknown. We aimed to develop an unsupervised method using multiple parameters from pre-operative diffusion tensor images for obtaining a clustered image that could enable visual grading of gliomas. Fourteen patients with low-grade gliomas and 19 with high-grade gliomas underwent diffusion tensor imaging and three-dimensional T1-weighted magnetic resonance imaging before tumour resection. Seven features including diffusion-weighted imaging, fractional anisotropy, first eigenvalue, second eigenvalue, third eigenvalue, mean diffusivity and raw T2 signal with no diffusion weighting, were extracted as multiple parameters from diffusion tensor imaging. We developed a two-level clustering approach for a self-organizing map followed by the K-means algorithm to enable unsupervised clustering of a large number of input vectors with the seven features for the whole brain. The vectors were grouped by the self-organizing map as protoclusters, which were classified into the smaller number of clusters by K-means to make a voxel-based diffusion tensor-based clustered image. Furthermore, we also determined if the diffusion tensor-based clustered image was really helpful for predicting pre-operative glioma grade in a supervised manner. The ratio of each class in the diffusion tensor-based clustered images was calculated from the regions of interest manually traced on the diffusion tensor imaging space, and the common logarithmic ratio scales were calculated. We then applied support vector machine as a classifier for distinguishing between low- and high-grade gliomas. Consequently, the sensitivity, specificity, accuracy and area under the curve of receiver operating characteristic curves from the 16-class diffusion tensor-based clustered images that showed the best performance for differentiating high- and low-grade gliomas were 0.848, 0.745, 0.804 and 0.912, respectively. Furthermore, the log-ratio value of each class of the 16-class diffusion tensor-based clustered images was compared between low- and high-grade gliomas, and the log-ratio values of classes 14, 15 and 16 in the high-grade gliomas were significantly higher than those in the low-grade gliomas ($p < 0.005$, $p < 0.001$ and $p < 0.001$, respectively). These classes comprised different patterns of the seven diffusion tensor imaging-based parameters. The results suggest that the multiple diffusion tensor imaging-based parameters from the voxel-based diffusion tensor-based clustered images can help differentiate between low- and high-grade gliomas.

Abbreviations: ADC, apparent diffusion coefficient; AUC, area under the curve; BET, FSL's Brain extraction Tool; BLSOM, batch-learning self-organizing map; CI, confidence interval; CNS, central nervous system; DTcl, diffusion tensor-based clustered image; DTI, diffusion tensor imaging; DWI, diffusion-weighted imaging; EPI, echo planar image; FA, fractional anisotropy; FDT, FMRIB's diffusion toolbox; FLAIR, fluid-attenuated inversion-recovery; FSL, FMRIB Software Library; HGG, high-grade glioma; KM, K-means; KM++, K-means++; L1, first eigenvalue; L2, second eigenvalue; L3, third eigenvalue; LGG, low-grade glioma; LOOCV, leave-one-out cross-validation; MD, mean diffusivity; MP-RAGE, magnetization-prepared rapid gradient-echo; MRI, magnetic resonance imaging; PET, positron emission tomography; ROC, receiver operating characteristic; ROI, region of interest; S0, raw T2 signal with no diffusion weighting; SOM, self-organizing map; SVM, support vector machine; T1WI, T1-weighted image; T1WIce, contrast-enhanced T1-weighted image; T2WI, T2-weighted image; WHO, World Health Organization.

* Corresponding author at: Human Brain Research Center, Kyoto University Graduate School of Medicine, 54 Kawahara-cho, Shogoin, Sakyo-ku, Kyoto 606-8507, Japan.
E-mail address: noishi@kuhp.kyoto-u.ac.jp (N. Oishi).

http://dx.doi.org/10.1016/j.nicl.2014.08.001

1. Introduction

Gliomas are the most common primary neoplasms of the central nervous system (CNS), and are classified according to a grading system, commonly that of the World Health Organization (WHO), on the basis of their histological appearance. Tumour grading is an important factor that influences the choice of therapy, such as adjuvant radiation and chemotherapy (Louis et al., 2007b).

Patients with low-grade gliomas (LGGs) (WHO grade II) may live for a long time, and the 5-year survival rate is 42%–92% (Sanai and Berger, 2008). In contrast, patients with high-grade gliomas (HGGs) (WHO grades III and IV) have a worst prognosis of brain tumours (Law et al., 2006); particularly, glioblastoma (WHO grade IV) develops rapidly (Ohgaki and Kleihues, 2007), and the 5-year survival rate is only 2% (McLendon and Halperin, 2003). Therefore, patients with HGGs need to be treated as soon as possible and more aggressively with chemotherapy and radiation. Thus, it is important to accurately classify gliomas into low or high grades to provide the best treatment for patients.

Magnetic resonance imaging (MRI) is essential for non-invasively diagnosing the existence, extent and characteristics of brain tumours. Different MRI sequences are used for evaluation and include T1-weighted image (T1WI), contrast-enhanced T1-weighted image (T1WIce), T2-weighted image (T2WI), diffusion-weighted imaging (DWI) and fluid-attenuated inversion-recovery (FLAIR) sequences. The images can provide much information about tumours, such as tumour morphology, the presence of enhancement, intra-tumoural haemorrhage or peri-tumoural oedema and can be helpful to predict tumour grade. The presence of contrast enhancement is often regarded as a sign of malignancy. Watanabe et al. reported that enhancement was present in 11 of 12 HGGs in their study, and histological examination revealed that areas of enhancement were related to neovascularity in tumour tissue or tumour cell infiltration (Watanabe et al., 1992). However, it was also reported that 9% of malignant gliomas lacked enhancement and 48% of LGGs were enhanced (Scott et al., 2002). These studies suggested that T1WIce was less useful than expected for prediction of glioma grade. Furthermore, gadolinium-based contrast agents, which are typically used in MRI, can cause side effects. Acute reactions after injection of gadolinium may cause flushing and nausea as minor reactions and hypotension and bronchospasm as intermediate reactions. In addition to these side effects, severe reactions are all symptoms of minor and intermediate reactions and sometimes cause cardiac arrest (Thomsen, 2003). Thus, T1WIce cannot be used for definitive pre-operative glioma grading because of insufficient information or side effects.

Some previous studies have used other MRI sequences without contrast agents, including diffusion tensor imaging (DTI), for glioma grading. Diffusion is sensitive to water movement, particularly along axonal fibres. DTI provides useful information about diffusion measurements and enables calculation of several parameters from DTI. Because tumour cells of gliomas mainly invade along white matter tracts (Scherer, 1938), we believe that DTI is a potentially useful sequence because of its sensitivity to white matter abnormalities (Filippi et al., 2001). Fractional anisotropy (FA) and apparent diffusion coefficient (ADC) calculated from DTI are more sensitive indicators of the integrity of white matter and tumour infiltration than are T1WI or T2WI (Price et al., 2003). Thus, DTI parameters can have an important role in the assessment of tumours. It has been reported that compared with white matter, HGGs show a mixture of hyper- and iso-intensities in DWI (Tien et al., 1994; Stadnik et al., 2001). One study found that lower ADC values corresponded to increased cellularity and HGGs (Kao et al., 2013). However, another study found no significant difference in ADC values between LGGs and HGGs (Lam et al., 2002). The FA values of LGGs were significantly lower than those of HGGs (Inoue et al., 2005; Kao et al., 2013), whereas another study showed low FA ratios in the tumour centres of both LGGs and HGGs (Goebell et al., 2006). These previous studies suggest that glioma grading with a single parameter of MRI remains controversial.

Recently, a pattern recognition method using multiple parameters has been applied to predict tumour grading. In a study, support vector machine (SVM), which is a widely used supervised machine-learning method because of its remarkable performance of classification, was applied and involved 161 features extracted from manually defined regions of interest (ROIs) on T1WI, T1WIce, T2WI, FLAIR and perfusion MRI using a contrast agent, and a combination of multiple features that differentiated HGGs and LGGs with an accuracy of 87.8%, sensitivity of 84.6% and specificity of 95.5% was reported (Zacharaki et al., 2009). Another study used a self-organizing map (SOM) based on a competitive learning algorithm, which is a type of neural network unsupervised learning, with seven features extracted from wavelet-filtered ADC, ADC, FLAIR and T2WI for each voxel (Vijayakumar et al., 2007). SOM was labelled for seven tissue classes, including low- and high-grade tumours, in a supervised manner using 700 voxel-based training pattern vectors. Although the sample size was small (four patients with low- and six with high-grade tumours), the method differentiated low-grade tumour from other tissues, with a sensitivity of 88% and a specificity of 98%, and high-grade tumour from other tissues, with a sensitivity of 87% and a specificity of 93%. Although pattern recognition methods with multiple parameters and a supervised manner can be useful for prediction of tumour grading, they have some problems in clinical applications. In voxel-based labelling, because it is impossible to examine the pathology of each voxel, supervised voxel-based labelling can be inaccurate and cause rater bias. Furthermore, complicated features make it difficult to determine the most sensitive parameter for characterizing grading. Therefore, a pattern recognition method with multiple uncomplicated parameters without supervised information can be helpful to predict glioma grade. Furthermore, SOM is well-known to its visualization and would help to lead to a novel classification.

This study aimed to develop a new method using multiple DTI-based parameters for voxel-based clustered images in an unsupervised manner that can be used to visually grade gliomas. We also determined if the method is really helpful for pre-operative prediction of glioma grade in a supervised manner.

2. Materials and methods

2.1. Subjects

We retrospectively reviewed 111 patients who were aged 6–87 years and had newly diagnosed and histologically confirmed diffusely infiltrative gliomas, defined according to the WHO classification (Louis et al., 2007a), between March 2010 and June 2013 in Kyoto University Hospital. We classified grade II as LGG ($n = 36$) and grades III and IV gliomas as HGG ($n = 75$) in this study. Patients with LGGs had 22 diffuse astrocytomas, eight oligodendrogliomas, four oligoastrocytomas and two mixed oligoastrocytoma. Patients with HGGs had 17 anaplastic astrocytomas, three anaplastic oligoastrocytomas, two anaplastic oligodendrogliomas and 53 glioblastomas. Among these patients, 51 underwent DTI and magnetization-prepared rapid gradient-echo (MP-RAGE). We excluded 13 patients who had undergone previous tumour resections or exposures to radiotherapy or chemotherapy prior to DTI acquisition. We also excluded three patients whose tumours were located around the temporal basal regions that were severely influenced by distortions of DTI (Mangin et al., 2002) and one patient because of appreciable motion artefacts in MP-RAGE. We excluded one patient <12 years of age because FA values in the frontal white matter are significantly lower in children aged 8–12 years than in adults because of less myelination in children (Klingberg et al., 1999). Consequently, 33 patients (22 men, 11 women) were enrolled in the study. Thirty-two patients had undergone tumour resections, and one had only undergone a biopsy. Twenty-one tumours were located in the frontal region, seven in temporal, two in parietal, one in occipital and two in frontoparietal (Table 1). This study was approved by the Ethics Committee of the Kyoto University Graduate School

Table 1
Summary of patient data.

Histopathology	n	WHO grade	Age (years)	Location
High-grade gliomas	19	III and IV	51.7 ± 18.6	
Glioblastoma	13	IV	54.1 ± 18.0	Frontal, parietal, temporal, frontoparietal
Anaplastic astrocytoma	4	III	33.5 ± 4.8	Frontal, temporal
Anaplastic oligoastrocytoma	2	III	72.0 ± 5.0	Frontal
Low-grade gliomas	14	II	42.7 ± 13.4	
Diffuse astrocytoma	6	II	47.5 ± 15.8	Frontal, parietal, frontoparietal
Oligoastrocytoma	3	II	40.3 ± 15.5	Frontal, temporal
Oligodendroglioma	4	II	38.0 ± 3.7	Frontal, temporal
Mixed oligoastrocytoma	1	II	40.0	Frontoparietal

Age (years) is given as means ± standard deviation.

of Medicine (C 570), and written informed consent was obtained from all patients.

2.2. MRI data acquisition and pre-processing

MRI images were scanned on a 3 Tesla Trio (Siemens, Erlangen, Germany) equipped with an eight-channel phased-array head coil.

DWI in an axial orientation used the following parameters: repetition time = 10,500 ms; echo time = 96 ms; flip angle = 90°; field of view = 192 × 192 mm; slices = 70; and voxel size = 2 × 2 × 2 mm. Diffusion weighting was isotropically distributed along 81 directions by using a b-value of 1500 s/mm^2 (Jones et al., 1999). Nine volumes with no diffusion weighting (b = 0 s/mm^2) were also acquired at points throughout acquisition. A set of diffusion-weighted data was acquired during a scanning time of approximately 18 min.

MP-RAGE using the following parameters was used to acquire three-dimensional T1-weighted anatomical images: repetition time = 2000 ms; echo time = 4.38 ms; flip angle = 8°; field of view = 176 × 192 mm; slices = 160; and voxel size = 1 × 1 × 1 mm. A dual-gradient field map in an axial orientation was also obtained by using the following parameters: repetition time = 511 ms; echo time 1/echo time 2 = 5.19/7.65 ms; flip angle = 60°; field of view = 192 × 192 mm; slices = 46; and voxel size = 3 × 3 × 3 mm.

DTI data were analysed using FSL [FMRIB Software Library v5.0.2.2, http://www.fmrib.ox.ac.uk/fsl (Smith et al., 2004)]. The data were corrected for eddy currents and head motion using affine registration to the first b = 0 reference volume. The data were also corrected for geometric distortions occurring in an echo planar image (EPI) (Jezzard and Balaban, 1995) by FUGUE, which is a part of the FSL tool for EPI correction of distortions caused by static magnetic field inhomogeneities (Jenkinson et al., 2012). Field inhomogeneities were measured by using a field-map image, and EPI was unwarped according to field-map data. Seven features, including DWI, FA, first eigenvalue (L1), second eigenvalue (L2), third eigenvalue (L3), mean diffusivity (MD) and raw T2 signal with no diffusion weighting (S0), were extracted from DTIs using the FMRIB's diffusion toolbox (FDT) program (Smith et al., 2004). The diffusivities derived from DTI measurements were separated into components parallel (L1) and perpendicular (L2 and L3) to the white matter tract. These components are referred to as MD, (L1 + L2 + L3)/3. FA, which assigns values between 0 and 1, represents how strongly water diffuses in the direction of the principal eigenvector (Holodny et al., 2001).

2.3. Feature extraction for clustering

The overview of the processing pipeline in the study is depicted in Fig. 1. The summary is as follows:

1 Feature extraction from DTI.
2 Clustering using SOM followed by K-means (KM).
3 Visualization of whole brain images by diffusion tensor-based clustering images (DTcIs).
4 Classification using DTcIs by SVM.

Features for unsupervised clustering were extracted from voxels on the seven intensity-normalized diffusion tensor images sampled at every 64 (4 × 4 × 4) voxels within the binary mask image obtained by FSL's Brain Extraction Tool (BET). The number of extracted features was 3552 ± 315 (mean ± SD) for each subject. The features of all subjects were then stacked and used for input vectors defined as $T = \{b_m, 1 \le m \le n\}$, where b_m is the mth vector and n is the number of vectors (117,232 in the study). The individual input vector (b_m) is defined as $b_m = [x_1, x_2, x_3, x_4, x_5, x_6, x_7]$, where $x_1, \ldots, x_7$ are components of the input vector. The components of each input vector (b_m) were extracted from DWI, ADC, MD, S0, L1, L2 and L3 images in the study.

2.4. Unsupervised clustering

The extracted feature vectors were used for calculating voxel-based clustered images. We applied the two-level clustering approach of SOM (Kohonen, 1995) and the KM algorithm (MacQueen, 1967) for unsupervised clustering (Fig. 1). First, a large number of input vectors were clustered into a much larger than the expected number of clusters, defined as 'protoclusters', by SOM. Then, the protoclusters were classified into the expected number of clusters, defined as 'clusters', by KM. The KM algorithm is a popular partition algorithm for clustering. Similar two-level clustering approaches have been reported (Chuang et al., 1999; Vesanto and Alhoniemi, 2000; Thomassey and Happiette, 2007) and applied in the fields of medicine (Wang et al., 2002) and others (Beccali et al., 2004; Lu et al., 2006). The two-level clustering approach has the following two important benefits compared with the KM algorithm,

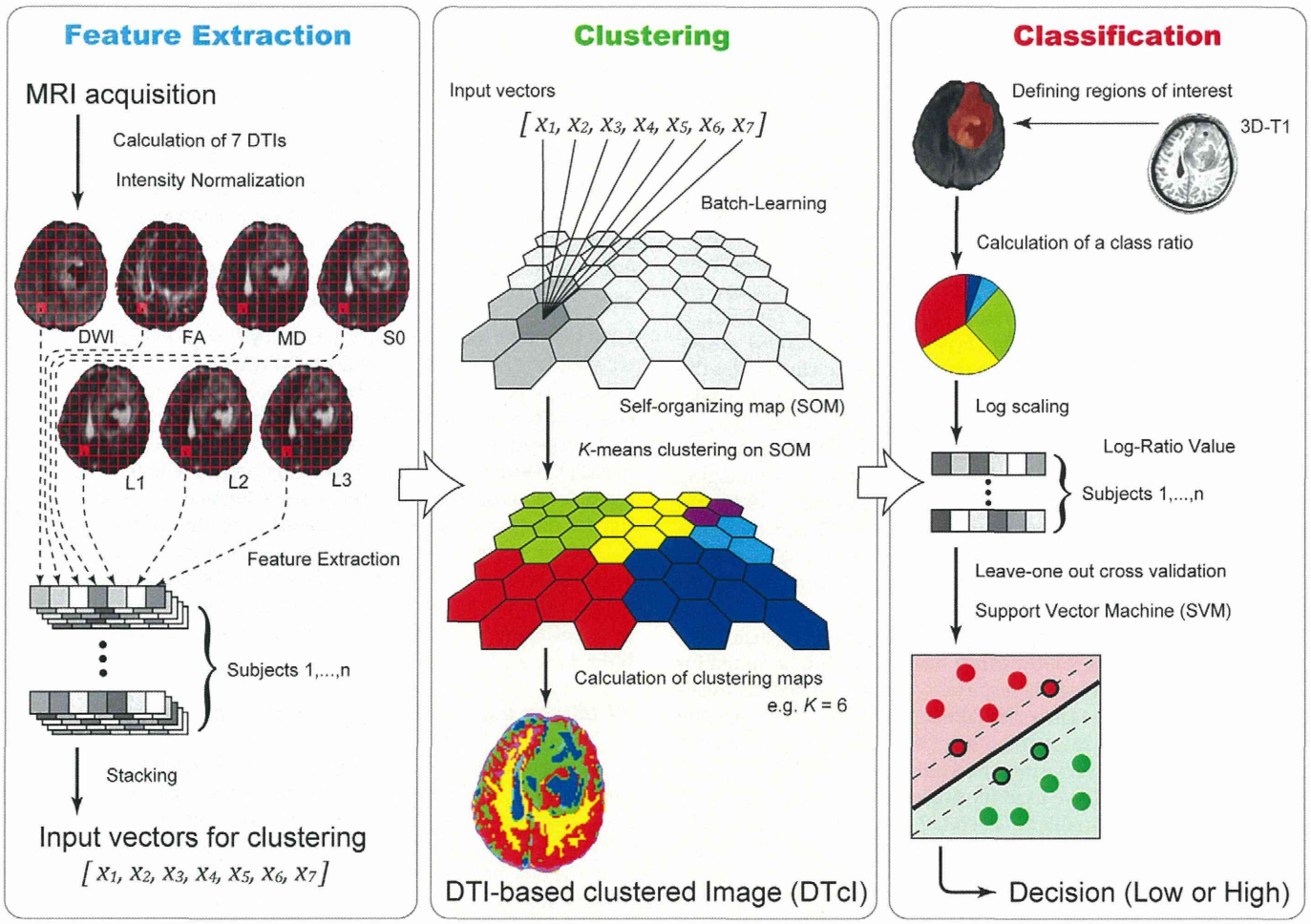

Fig. 1. Simplified graphical overview of the processing pipeline.

which is one of the most famous and effective unsupervised clustering approaches: One is noise reduction. It is known that the KM algorithm is very sensitive to outliers (Velmurugan and Santhanam, 2010). Because protoclusters are local averages of the input vectors and outliers can be filtered out, they are more robust to outliers than are the original vectors. The other is the reduction of the computational cost. Furthermore, the two-dimensional arrangement of the larger protoclusters by SOM can be easily visualized, thus, providing useful information about the features (Jin et al., 2004).

2.4.1. Unsupervised clustering: SOM

SOM is based on a competitive learning algorithm, which is a type of neural network unsupervised learning. It typically comprises hexagonal and two-dimensional grids of map units (also called neurons) defined as $H = \{w_i;\ 1 \le i \le K \times L\}$. Here, K and L are the numbers of columns and rows, respectively, w_i represents the weight vectors assigned to the ith unit of the SOM architecture, defined as $w_i = [v_1,\ldots,v_d]$, where d is the dimension of the weight and $v_1,\ldots,v_d$ are components of the weight vector. The dimension of the weight vector was seven in this study.

A major problem in the standard sequential SOM algorithm is that the results differ according to the input order. Therefore, the batch-learning algorithm for the SOM (batch-learning self-organizing map; BLSOM) (Kohonen, 1995) was used in the study. The results by BLSOM are consistent because its learning does not depend on the input order. Other advantages of BLSOM compared with the standard sequential SOM are that no learning rate has to be specified by the user of the algorithm and convergence of the input vectors is faster towards their final values (Brugger et al., 2008). The following algorithm was used for BLSOM:

1 Initialize the weight vectors $w_i(0)$ of all map units.
2 Calculate the Voronoi sets $V_i(t) = \{b \mid d(b_j, w_i(t)) < d(b_j, w_k(t))\forall_{k\neq i}\}$ and the sums $s_i(t) = \sum_{j=1}^{|V_i(t)|} b_j$.
3 Update the weight vectors according to $w_i(t+1) = \sum_j h_{ij}(t)s_j(t) / \sum_j |V_i(t)|h_{ij}(t)$.
4 Repeat steps 2 and 3 until a predefined number of steps τ.

Here, $w_i(t)$ is a weight vector in the tth step and $h_{ij}(t)$ is the neighbourhood function defined by $h_{ij}(t) = exp(-||r_i - r_j||^2/2\sigma^2(t))$, where r_i and r_j are the ith and jth units of the SOM architecture, respectively, $||r_i - r_j||$ denotes the Euclidean distance between r_i and r_j, and $\sigma(t)$ is the neighbourhood radius defined by $\sigma(t) = \sigma_{final} + (\sigma_{initial} - \sigma_{final})(1 - t/\tau)$, where $\sigma_{initial}$ and σ_{final} are the neighbourhood radii in the initial and final steps, respectively. In the study, the initial weight vectors $w_i(0)$ in step 1 were defined on the basis of principal component analysis of the input vectors b_m by $w_i(0) = \bar{b} + 10s_1\{(k-K/2)/K\}a_1 + 10s_2\{(l-L/2)/L\}a_2$, where $\bar{b}$ is the average vector of b_m, a_1 and a_2 are the eigenvectors of the first and second principal components and s_1 and s_2 are the standard deviations of the first and second principal components. k and l are the kth column and lth row in the ith unit of the SOM architecture, respectively. The parameters for BLSOM used in the study were defined as $K = 20$, $L = 20$, $\sigma_{initial} = 3.0$, $\sigma_{final} = 2.0$ and $\tau = 100$ based on the previous studies. Vijayakumar et al. used SOM for segmentation of brain tumour on MRI with pre-defined